KCL-MTH-15-08

Box Graphs and Resolutions II:

From Coulomb Phases to Fiber Faces

Andreas P. Braun [1] and Sakura Schäfer-Nameki [2]

[1] *Rudolf Peierls Centre for Theoretical Physics, University of Oxford*
Oxford, OX1 3NP, UK
[1] *Mathematical Institute, University of Oxford,*
Oxford, OX2 6GG, UK
[2] *Department of Mathematics, King's College London*
The Strand, London WC2R 2LS, UK
gmail: andreas.braun.physics, sakura.schafer.nameki

arXiv:1511.01801v1 [hep-th] 5 Nov 2015

Box graphs, or equivalently Coulomb phases of three-dimensional $N = 2$ supersymmetric gauge theories with matter, give a succinct, comprehensive and elegant characterization of crepant resolutions of singular elliptically fibered varieties. Furthermore, the box graphs predict that the phases are organized in terms of a network of flop transitions. The geometric construction of the resolutions associated to the phases is, however, a difficult problem. Here, we identify a correspondence between box graphs for the gauge algebras $\mathfrak{su}(2k+1)$ with resolutions obtained using toric tops and generalizations thereof. Moreover, flop transitions between different such resolutions agree with those predicted by the box graphs. Our results thereby provide explicit realizations of the box graph resolutions.

Contents

1 Introduction **3**

2 Box Graphs, Coulomb Phases and Fibers **5**

2.1 Coulomb Phases for $\mathfrak{su}(2k+1)$ with $\Lambda^2 V$ Matter 5

2.2 Coulomb Phases for $\mathfrak{su}(2k+1)$ with $\Lambda^2 V \oplus V$ Matter 7

2.3 Fibers from Coulomb Phases/Box Graphs 8

3 Toric Resolutions, Tops and Weighted Blowups **10**

3.1 Weighted Blowups 11

3.2 Toric Calabi-Yau Hypersurfaces 11

3.3 Tops and Elliptic Fibrations 12

3.4 Triangulations of Tops and Fiber Faces 14

3.5 Flops 15

4 Fiber Faces and Box Graphs for $\mathfrak{su}(2k+1)$ **16**

4.1 Tate Resolution 16

4.2 Algebraic Resolutions and Hypercubes 18

4.3 Fiber Face Triangulations 19

4.4 Coulomb Phases/Box Graphs for Triangulations of Tops 23

5 Secondary Fiber Faces and Complete Intersections **28**

5.1 Blowdowns and Elementary Flops 29

5.2 Complete Intersections and Secondary Fiber Faces 33

5.3 Coulomb Phases/Box Graphs for Secondary Fiber Faces 36

6 Generalized Fiber Faces from Box Graph Layers **38**

6.1 Flops to the next Layer 38

6.2 Conjecture on Layer Structure 40

7 Discussion and Outlook **42**

A Number of Triangulations of a Strip **43**

B Fibers and Phases for $\mathfrak{su}(7)$ **44**

B.1 Box Graphs 45

B.2 Fiber Faces and Weighted Blowups 46

B.3 Blowdowns and Flops 51

1 Introduction

Beyond its applications in the modeling of particle physics and classification of 6d superconformal field theories, recent developments in F-theory have led to tremendous progress in uncovering properties of higher-dimensional elliptically fibered complex varieties. Much of the progress has been made in particular in the study of crepant resolutions of singular elliptic fibers in higher dimensional varieties, i.e. resolutions that keep the canonical class unchanged.

The canonical setup of interest in F-theory compactifications [1] is an elliptically fibered Calabi-Yau variety in dimension 3 and 4, which models $N = (1, 0)$ six dimensional or four-dimensional $N = 1$ supersymmetric field theories, with gauge algebra $\mathfrak{g}$, and matter in the representations $\mathbf{R}_i$ of $\mathfrak{g}$. Four-folds in addition allow for codimension three singularities, where Yukawa couplings are realized. The F-theory limit is obtained by taking the volume of the fiber to zero, and this singular limit is in fact not sensitive to which crepant resolution is used [2,3]. However, various more refined aspects of the F-theory compactification, such determining the G_4-flux, the possible $U(1)$ and discrete symmetries, make use of the singularity resolutions.

By Kodaira's classification of singular fibers, one can associate a Lie algebra $\mathfrak{g}$ to an elliptic fibration. These are characterized in terms of an ADE type affine Dynkin diagram representing the dual graph to the intersection graph of the rational curves in the singular fiber. This classification holds for all singular fibers over codimension one loci in the base. In higher codimension, this classification ceases to be comprehensive, and additional structures emerge that are required in order to characterize how higher codimension singular fibers can occur, and what their characterization is.

In [4] (see also [5–9]), inspired by the correspondence to classical Coulomb phases in 3d and 5d supersymmetric gauge theories [10–14,5], a proposal was put forward to systematically describe the distinct small resolutions of singular elliptic fibrations, including fibers in codimension two and three. In addition to a Lie algebra $\mathfrak{g}$, which characterizes the codimension one fibers, the codimension two fibers have a representation $\mathbf{R}$ of $\mathfrak{g}$ associated to them, and by [4], the fibers can be obtained by a decorated representation graph, or box graph. Flops between distinct small resolutions are realized by the action of a quotiented Weyl group. Note that the box graphs are motivated from a dual M-theory compactification point of view and map the problem of small resolutions to Coulomb phases. However, as shown in [4], the analysis applies directly in the cone of effective curves of the elliptic fibration, and does not require any reference to the gauge theory. Recently, this work was utilized in [7] to de-

termine a classification of the fibers in codimension two with additional $U(1)$ symmetries, which geometrically are realized in terms of rational sections. This has led to a survey of all F-theory Grand Unified Theories (GUTs) with additional $U(1)$ symmetries, with interesting phenomenological implications [15]. Thus the results on codimension two fibers are not merely of mathematical relevance, but indeed have far-reaching implications for the particle physics, in particular flavor properties, of F-theory compactifications.

Beyond this abstract characterization of elliptic fibrations, much progress has been made in the direct realization of elliptic curves in terms of hypersurfaces or complete intersections, for instance in toric varieties [16–23]. What is apparent from all these resolutions is that neither toric, nor algebraic resolutions necessarily yield the full set of possible fibers predicted in [4]. Concrete realizations of the complete set of distinct resolutions have indeed been determined for $\mathfrak{su}(5)$ in [5, 6, 9], with both fundamental and anti-symmetric matter, in terms of resolutions of the Tate model for a codimension one I_5 Kodaira fiber [24, 25].

The purpose of the present work is to clarify the connection between toric and algebraic resolutions on the one hand, and the more general resolutions that are predicted by the box graphs, on the other. We will determine a characterization of all algebraic resolutions in terms of a subclass of box graphs, which have a simple combinatorial description. Furthermore, resolutions associated to triangulations of toric tops [26] are determined in terms of triangulations of a so-called *fiber face*. We then show how fiber face triangulations form a subset of the box graph resolutions and determine a one-to-one map between these for $\mathfrak{su}(n)$ gauge algebras with anti-symmetric representation. The fate of fiber components when approaching these matter loci can be easily read off the fiber face triangulation. The resulting correspondence also provides an identification between the flops of the fiber face triangulations and single box sign changes in the box graphs.

Beyond the class of fiber face triangulations originating from toric tops, which are the subject of section 4, we determine a class of resolutions realizing the fiber as a complete intersection. Likewise, these have a succinct characterization in terms of triangulations of what we call a *secondary fiber face*. This again has a simple characterization in terms of box graphs as shown in section 5. This structure is then extended to a third layer, and we conjecture that it persists for all remaining phases in section 6.2.

The correspondence between box graphs and fiber face triangulations is exemplified in the context of $\mathfrak{su}(7)$ with anti-symmetric representation $\mathbf{R} = \mathbf{21}$, where each of these box graph layers is discussed in detail and the corresponding resolutions (which in this case is the complete set) are determined in appendix B. We conclude with a discussion of extensions and applications of our results in section 7.

2 Box Graphs, Coulomb Phases and Fibers

Consider a singular elliptic fibration, with trivial canonical class, and a base of dimension at least two. Let $\mathfrak{g}$ be the Lie algebra associated to the singular fibers, i.e. the intersection graph of the exceptional curves of the singular Kodaira fibers are given in terms of the affine Dynkin diagram of $\mathfrak{g}$. The fibers in codimension two, associated to a representation $\mathbf{R}$ of $\mathfrak{g}$, can be characterized in terms of box graphs, introduced in [4], which are a combinatorial, graphic presentation of the codimension two fibers, which are based on the representation graph $\mathbf{R}$.

This section is a review of the results obtained in [4], and developed further in [7], with a focus on the anti-symmetric representation $\Lambda^2 V$ for $\mathfrak{su}(2k+1)$. The codimension one fibers for this setup are of Kodaira type I_{2k+1}, corresponding to an $\mathfrak{su}(2k+1)$ gauge algebra. In codimension two, the rational curves in the fiber intersect according to Kodaira type I^*_{2k-3}, which realize matter in the anti-symmetric representation $\Lambda^2(\mathbf{2k+1})$. However, in this case there are inequivalent topological realizations. These are obtained by resolutions of Weierstrass or Tate models and, depending on which resolution is carried out, different components of the I_{2k+1} fiber become reducible in codimension two. The box graphs provide an elegant characterization of all resolutions, but do not provide a constructive way to realize these geometrically. One of the goals of this paper is to determine the corresponding resolutions.

2.1 Coulomb Phases for $\mathfrak{su}(2k+1)$ with $\Lambda^2 V$ Matter

Let us begin with the discussion of (classical) Coulomb phases for $\mathfrak{su}(2k+1)$ with matter in the anti-symmetric representation and their succict characterization in terms of Box graphs. To begin with, let $\mathfrak{g} = \mathfrak{su}(2k+1)$ and let L_i, $i = 1, \cdots, 2k+1$ be its fundamental weights. With the constraint that $\sum_i L_i = 0$, the simple roots can be represented as

$$\alpha_i = L_i - L_{i+1}\,, \qquad i = 1, \cdots, 2k\,. \tag{2.1}$$

The weights of the antisymmetric representation of dimension $(2k+1)k$ are

$$L_{ij} = L_i + L_j\,, \qquad i < j\,. \tag{2.2}$$

The representation graph for a representation $\mathbf{R}$ is defined in terms of boxes, which correspond to the weights of $\mathbf{R}$. These are arranged in such a way that adjoining walls represent the action of simple roots within the representation. The representation graph for $\Lambda^2(\mathbf{2k+1}) = \Lambda^2 V$ is shown in figure 1.

The singular fibers in codimension two can be equally characterized in terms of the Coulomb branch phases of an $N = 2$ supersymmetric gauge theory in $d = 3$ (or $d = 5$

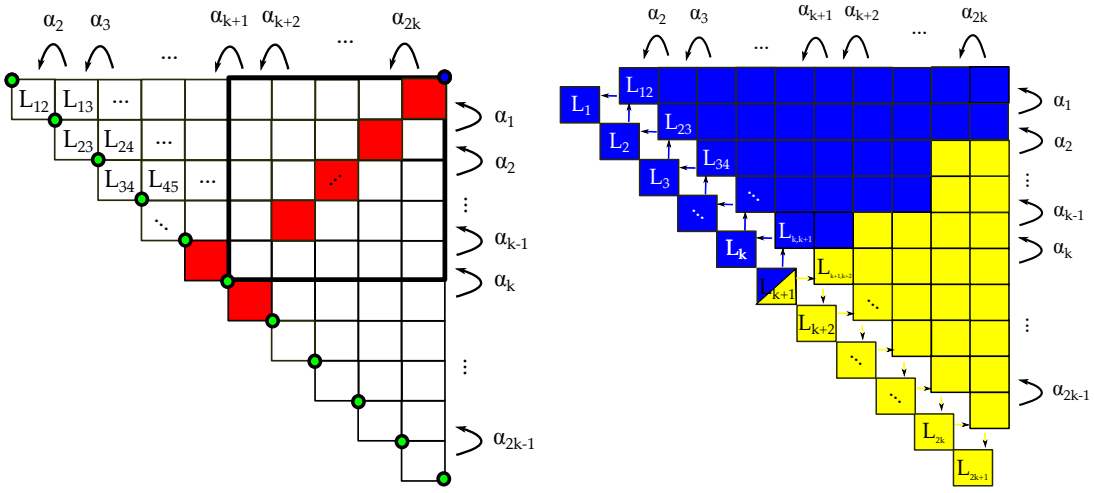
α2 α3 ... αk+1 αk+2 ... α2k
L12 L13 ...
L23 L24 ...
L34 L45 ...
α1 α2 αk-1 αk α2k-1
α2 α3 ... αk+1 αk+2 ... α2k
L1 L12 L2 L23 L3 L34 Lk Lk+1 Lk+2 L2k L2k+1
α1 α2 αk-1 αk α2k-1

Figure 1: The left hand side shows the representation graph for the anti-symmetric representation of $\mathfrak{su}(2k+1)$ with weights $L_{ij} = L_i + L_j$ with $i < j$. The red boxes correspond to the diagonal $\mathcal{E}_{2k+1}$, defined in (2.5). The right hand side shows a Box Graph for matter in the combined anti-symmetric and fundamental representation of $\mathfrak{su}(2k+1)$, with $\pm$ shown in blue/yellow. The NW-SE additional diagonal corresponds to the box graph of the fundamental representation with weights L_1 to L_{2k+1}. The blue/yellow arrows indicate the flow rules between fundamental and anti-symmetric representation. For this box graph corresponding to the anti-symmetric representation, there are two box graphs consistent with the flow rules for the fundamental representation. These are distinguished by choosing $\epsilon(L_{k+1}) = \pm$.

depending on whether the elliptic fibration is a four-fold or three-fold) with chiral matter in the representation $\mathbf{R}$. Geometrically, this means that the singular fiber degenerates further in codimension two, and the singularity can be characterized in terms a higher rank Lie algebra $\widetilde{\mathfrak{g}}$. Higgsing the adjoint of this algebra $\mathfrak{g}$ gives rise to bifundamental matter[1]

$$\begin{aligned} \widetilde{\mathfrak{g}} \quad &\to \quad \mathfrak{g} \oplus \mathfrak{u}(1) \\ \mathrm{Adj}(\widetilde{\mathfrak{g}}) \mapsto \quad &(\mathrm{Adj}(\mathfrak{g}), \mathbf{1}) \oplus (\mathbf{1}, \mathrm{Adj}(\mathfrak{u}(1))) \oplus (\mathbf{R}, +1) \oplus (\overline{\mathbf{R}}, -1)\,. \end{aligned} \tag{2.3}$$

The key insight of [4] is that Coulomb phases, and thereby singular fibers in codimension two, are characterized in terms of box graphs $\mathcal{B}^{\mathbf{R}}_{\epsilon}$, i.e. a sign-decorated representation graphs of $\mathbf{R}$, where the signs are given by a map

$$\epsilon : \mathrm{Weights}(\mathbf{R}) \quad \to \quad \{\pm\}\,, \qquad \epsilon(L_{ij}) = \pm\,, \tag{2.4}$$

satisfying a set of conditions, which e.g. for $\mathfrak{su}(2k+1)$ with $\mathbf{R} = \Lambda^2(\mathbf{2k+1})$ are

[1]The case of a non-abelian commutant of $\mathfrak{g}$ in $\widetilde{\mathfrak{g}}$ was discussed also in [4], and has very interesting properties. Here we are only interested in the case of an abelian commutant.

(1.) Flow rules for the anti-symmetric representation:
If $\epsilon(L_{ij}) = +$ then $\epsilon(L_{kl}) = +$ for all (k,l) with $k \leq i$ and $l \leq j$.
If $\epsilon(L_{ij}) = -$ then $\epsilon(L_{kl}) = -$ for all (k,l) with $k \geq i$ and $l \geq j$.

(2.) Trace condition for the anti-symmetric representation:
Let $\mathcal{E}_{2k+1} = \{\epsilon(L_{1,2k+1}), \epsilon(L_{2,2k}), \cdots, \epsilon(L_{k-1,k+3}), \epsilon(L_{k,k+1}), \epsilon(L_{k+1,k+2})\}$. Then

$$\mathcal{E}_{2k+1} \neq (+, \cdots, +) \qquad \text{and} \qquad \mathcal{E}_{2k+1} \neq (-, \cdots, -)\,. \tag{2.5}$$

The flow rules ensure that if two weights are related by the action of a positive root, then their sign assignment needs to be the same. The trace condition says that the weights on the 'diagonal' defined in terms of $\mathcal{E}_{2k+1}$ cannot all have the same sign. This ensures that we obtain an $\mathfrak{su}(2k+1)$ phase, rather than a $\mathfrak{u}(2k+1)$ one. The diagonal is shown in figure 1 in terms of the red boxes.

The sign assignment is uniquely characterized in terms of the path separating the + and − signed boxes, starting at the upper right hand corner (blue point in figure 1), and ending on one of the points on the NW-SE diagonal (one of the green points in figure 1). These are so-called anti-Dyck path associated to the box graph. As an example, in figure 15 all the phases of $\mathfrak{su}(7)$ with the anti-symmetric representation **21**, including the anti-Dyck paths, are shown.

Flop transitions between two phases are defined as single-box sign changes which map between two consistent phases, both satisfying (1.) and (2.). Geometrically, these correspond exactly to flop transitions in the codimension two fibers. One of the goals of this paper is to realize these concretely in a geometric setting, such as a toric realization of the singular fibers. The flop network for $\mathfrak{su}(7)$ is shown in figure 15.

2.2 Coulomb Phases for $\mathfrak{su}(2k+1)$ with $\Lambda^2 V \oplus V$ Matter

Although the main concern of this paper is the anti-symmetric representation, we will make several references to the Coulomb phases and box graphs for the fundamental representation as well. The weights for the $\mathbf{2k+1}$ fundamental representation are L_i, $i = 1, \cdots, 2k+1$, with $\sum L_i = 0$. The phases can again be mapped to representation graphs with a sign decoration $\epsilon : \mathbf{R} \to \pm 1$, satisfying a set of flow rules and trace condition:

(1.) Flow rules for the fundamental representation:
If $\epsilon(L_i) = +$ then $\epsilon(L_j) = +$ for all $j < i$.
If $\epsilon(L_i) = -$ then $\epsilon(L_j) = -$ for all $j > i$.

(2.) Trace condition for the fundamental representation: The signs cannot be all + or all −.

Furthermore, the phases for the combined anti-symmetric and fundamental representations are obtained by combining the phase of the fundamental and anti-symmetric [4, 6] such that

(AF0.) The phases for each representation separately are consistent $\mathfrak{su}(2k+1)$ phases.

(AF1.) Flow rules for combined anti-symmetric and fundamental representation:

$$\begin{aligned} \epsilon(L_i) = + \quad &\Rightarrow \quad \epsilon(L_{i-1,i}) = + \\ \epsilon(L_{i,i+1}) = + \quad &\Rightarrow \quad \epsilon(L_i) = + \\ \epsilon(L_i) = - \quad &\Rightarrow \quad \epsilon(L_{i,i+1}) = - \\ \epsilon(L_{i,i+1}) = + \quad &\Rightarrow \quad \epsilon(L_{i+1}) = - \,. \end{aligned} \tag{2.6}$$

One can determine the corresponding box graphs by attaching the fundamental representation along the NW to SE diagonal to the anti-symmetric box graph. The resulting graph then needs to satisfying the flow rules, viewed as a box graph for $\mathfrak{su}(2k+2)$ with the anti-symmetric representation. This is shown in figure 1.

2.3 Fibers from Coulomb Phases/Box Graphs

The box graphs give a succinct characterization of all the small resolutions of singular Weierstrass models. First we introduce the notion of a relative cone of effective curves (see e.g. [27]). Let X be a projective variety. Then the group of Cartier divisors is

$$N^1(X) = \{D \text{ Cartier divisor in } X\}/\sim , \tag{2.7}$$

where $\sim$ corresponds to numerical equivalence, i.e.

$$D \sim D' \;\text{ if }\; D \cdot C = D' \cdot C \;\text{ for all }\; C \in H_2(X, \mathbb{Z}) \,. \tag{2.8}$$

Two curves are numerically equivalent $C \sim C'$, if their intersections with any element in $N^1(X)$ agrees, and we correspondingly define $N_1(X)$ as the quotient of all (complex) 1-cycles by numerical equivalence. Any 1-cycle in X can be written as a formal integral sum $\sum_i n_i C_i$, with $n_i \in \mathbb{Z}$, where C_i are integral curves in X (i.e. actual subspaces of complex dimension 1 in X). A curve is called *effective* if all coefficients n_i are non-negative.

In $N_1(X)$ the effective curves form a convex cone, denoted by $NE(X)$.

Definition 2.1 *Let X and Y be two projective varieties and $\pi : X \to Y$ a morphism. Then the relative cone of curves $NE(\pi)$ of the morphism π is the convex subcone of the cone of effective curves $NE(X)$, generated by the curves that are contracted by π.*

Let X be a smooth elliptically fibered Calabi-Yau variety of dimension n, with a section, and let

$$\pi : \quad X \ \rightarrow \ Y \tag{2.9}$$

be the contraction of all rational curves in the fiber which do not meet the zero section, so that Y is the singular Weierstrass model associated to X. This definition of a singular limit [2,3] is the relevant one for F-theory. We can associate to a singular Weierstrass model with Kodaira fibers in codimension one in the base a Lie algebra $\mathfrak{g}$ [2]. In codimension two, the singularity can enhance, which associates a representation $\mathbf{R}$ to the fibers. In [4,7] it was shown that $NE(\pi)$ for this map π can be constructed using the box graphs, and for a given singular Weierstrass model Y, all the smooth models X_i, with singular limits π_i, which are related by flop transitions, were determined:

Fact 2.1 (Box Graphs and Resolutions) *Let Y be a singular Weierstrass model of dimension at least three, with codimension one singularity associated to a Lie algebra $\mathfrak{g}$ and codimension two singularities associated to a representation $\mathbf{R}$ of $\mathfrak{g}$. There is a one-to-one correspondence between box graphs $\mathcal{B}^{\mathbf{R}}_{\epsilon^{(i)}}$ – associated to a representation $\mathbf{R}$ and a sign assignment $\epsilon^{(i)}$: weights$(\mathbf{R}) \rightarrow \pm 1$ – and a pair (X_i, π_i) of smooth elliptic Calabi-Yau varieties, with maps $\pi_i : X_i \rightarrow Y$. In particular, the cone $NE(\pi_i)$ can be characterized in terms of the box graphs as follows*

$$NE(\pi_i) = \left\langle \{F_i, i = 0, \cdots, rank(\mathfrak{g})\} \cup \{C_w \, , w \in \mathbf{R} : \ \exists j : \ \mathcal{B}^{\mathbf{R}}_{\epsilon^{(j)}} = \mathcal{B}^{\mathbf{R}}_{\epsilon^{(i)}}|_{\epsilon^{(j)}(w) = -\epsilon^{(i)}(w)} \} \right\rangle_{\mathbb{Z}} . \tag{2.10}$$

Here, F_i are the rational curves associated to the simple roots of $\mathfrak{g}$, and C_w are the rational curves associated to weights w of the representation $\mathbf{R}$. The extremal generators of these cones, and flop transitions between two smooth models (X_i, π_i), can be determined as follows, see Facts 2.2 and 2.3 in [7]:

Fact 2.2 (Flops and Extremal Rays) *Single box sign changes that map between box graphs $\mathcal{B}^{\mathbf{R}}_{\epsilon^{(i)}}$ correspond to flop transitions between the geometries X_i. The convex cones $NE(\pi_i)$ can be written in terms of extremal rays*

$$NE(\pi_i) = \bigoplus_k \mathbb{Z}^+ \ell_k \, , \tag{2.11}$$

where ℓ_k are the generators of the extremal rays, given by:

[2] We focus our attention here to the I_n and I_n^* as well as II^*, III^*, IV^*, with associated gauge algebras $\mathfrak{su}(n)$, $\mathfrak{so}(2n)$, and $\mathfrak{e}_n$.

(1.) F_i, *associated to the simple roots of* $\mathfrak{g}$ *are extremal generators, is extremal if the anti-Dyck path of* $\mathcal{B}^{\mathbf{R}}_{\epsilon^{(i)}}$ *does not cross the horizontal or vertical lines in the box graph, which correspond to adding the simple root* α_i,

(2.) $\epsilon^{(i)}(w)C_w$ *is extremal if there exists* j *such that* $\mathcal{B}^{\mathbf{R}}_{\epsilon^{(j)}} = \mathcal{B}^{\mathbf{R}}_{\epsilon^{(i)}}|_{\epsilon^{(j)}(w)=-\epsilon^{(i)}(w)}$.

The condition (1.) essentially states that F_i is extremal if it stays irreducible in codimension two. The second condition states that a rational curve associated to a weight w is extremal if it can be flopped, i.e. changing its sign gives rise to another consistent phase. The extremal generators of $NE(\pi_i)$ correspond to the fiber components of the codimension two fiber, and we will explain the construction of this when discussing the toric fibers. In section 4.4 we will provide more details on the precise identification of Coulomb Phases/Box Graphs, with fiber components.

The characterization of crepant resolutions of elliptic Calabi-Yau varieties in terms of box graphs is very elegant and concise, however it does not give a constructive way of determining the resolutions X_i of the singular Weierstrass models Y. The main purpose of this paper is to show how such resolutions can be geometrically realized. We continue now with a brief summary of various toric tools, which will be useful in this process.

3 Toric Resolutions, Tops and Weighted Blowups

To keep this paper reasonably self-contained, we collect some background on the toric resolution techniques to be used below and set up notations and conventions. A more in-depth treatment tailored to our needs can be found in [6], see also [28–32] for basic definitions and properties concerning toric varieties and their Calabi-Yau submanifolds.

Given a (appropriate) fan[3] Σ, there is an associated (smooth, projective) toric variety T_Σ. A special role is played by the generators of the rays ρ_i (one-dimensional cones in Σ), which we denote by v_i. For every v_i there is an associated homogeneous coordinate z_i and a toric divisor D_i. The fan Σ encodes the linear relations between the divisors D_i as well as their intersections.

We may describe T_Σ as the quotient

$$T_\Sigma = \left(\mathbb{C}^{n+k} \setminus Z\right) / \left((\mathbb{C}^*)^k \times G\right) . \tag{3.1}$$

[3]As usual, we assume that one starts with dual lattices N and M. The fan Σ sits inside $N \otimes \mathbb{R}$ and is rational (with respect to N), polyhedral, strongly convex and simplicial. If there is a strongly convex piecewise linear support function on Σ, the corresponding toric variety is projective. See e.g. [29] for explanations of these terms. As is customary in the literature, we denote the dual lattice to N by M and the product between elements of the two lattices by $\langle M, N\rangle$.

The Stanley-Reisner (SR) ideal Z contains all collections of homogeneous coordinates $\{z_i\}$ for which the corresponding rays $\{\rho_i\}$ do not share a common cone in Σ. The weights s_i of the $\mathbb{C}^*$ actions which are modded out can be found from relations of the form

$$\sum s_i v_i = 0\,. \tag{3.2}$$

Finally, the finite group G is isomorphic to the quotient N/N_v, where N_v is the lattice spanned by all v_i in Σ.

3.1 Weighted Blowups

Refinements $\Sigma' \to \Sigma$ of the fan induce birational maps $T_{\Sigma'} \to T_\Sigma$, i.e. we may think of them as (generalized) blowups. In particular, refinements in which we introduce a single new ray v_E into Σ correspond to weighted blowups according to the following rules. Let us assume that v_E sits in the interior of a d-dimensional cone σ, generated by $\{v_1, \cdots, v_d\}$. The introduction of v_E means we have to subdivide σ into the cones

$$\langle v_1, \cdots, v_d\rangle \to \langle v_1, \cdots v_E\rangle, \cdots, \langle v_E, \cdots v_n\rangle\,. \tag{3.3}$$

For $d < n$, we also have to accordingly subdivide all higher-dimensional cones containing σ as a face. On the level of the description (3.1), the upshot of such a refinement is that the SR-ideal of Z now contains the relation $z_1 = \cdots = z_d = 0$. Furthermore, v_E being contained in the interior of σ means that we may write

$$\sum_i a_i v_i = a_E v_E\,, \tag{3.4}$$

so that there is a new $\mathbb{C}^*$ action with the corresponding weights in $T_{\Sigma'}$. If all of the weights $a_i = 1$ and $a_E = 1$, this fan refinement is equivalent to a standard algebraic blowup $(z_1, \cdots, z_d; z_E)$, where the notation means that the locus $z_1 = \cdots = z_d = 0$ gets resolved with new exceptional section z_E (see section 4.1 for more details). In general, we can think of such a refinement as a weighted blowup with weights a_i and a_E.

3.2 Toric Calabi-Yau Hypersurfaces

The anti-canonical class of T_Σ can be expressed as

$$-K = \sum_i D_i\,. \tag{3.5}$$

A Calabi-Yau hypersurface is hence described by taking the zero locus of a section $P(z_i)$ of the corresponding line bundle. Calabi-Yau hypersurfaces in compact toric varieties can be

described by means of pairs of reflexive polytopes, see [31] for a lightning review. Here, all rays of Σ are generated by vectors v_i on the surface of an N-lattice polytope Δ°, which is called reflexive if its polar dual Δ, defined by

$$\langle \Delta, \Delta^\circ \rangle \geq -1\,, \tag{3.6}$$

is a lattice polytope as well (in the dual lattice M). While the N-lattice polytope Δ° gives rise to the fa**N**, the **M**onomials of a generic hypersurface equation $P(z_i) = 0$ are determined by the M-lattice polytope Δ. Every point m on Δ gives rise to a monomial

$$P(z_i) \supset c_m \prod_i z_i^{\langle m, v_i\rangle + 1}\,. \tag{3.7}$$

This presentation allows for a convenient resolution of singularities: if we are given a singular Calabi-Yau hypersurface defined by a set of monomials with generic coefficients, which lie on a (Newton) polytope Δ, we automatically get a crepant (partial) resolutions by performing toric resolutions for which all of the new rays in $\Sigma(1)$ are points on Δ°.

More generally, one may construct a maximal smooth ambient toric variety (and thereby a maximally smooth hypersurface) by considering a fine triangulation of Δ° and simply taking all cones over the simplices on the boundary of Δ°. In this case, not all lattice points on Δ° necessarily give rise to divisors on a Calabi-Yau hypersurface: divisors corresponding to points interior to maximal-dimensional faces of Δ° miss any smooth Calabi-Yau hypersurface.

3.3 Tops and Elliptic Fibrations

In the present context we are not interested in Calabi-Yau hypersurfaces per se, but rather elliptic Calabi-Yau manifolds for which the elliptic fiber is described by a Tate model. This means that we can describe the elliptic fiber by a hypersurface equation

$$y^2 + yxwb_1 + yw^3b_3 = x^3 + x^2w^2b_2 + xw^4b_4 + w^6b_6\,, \tag{3.8}$$

in the weighted projective space $\mathbb{P}_{123}$. The whole elliptic Calabi-Yau manifolds is then obtained by fibering $\mathbb{P}_{123}$ over a base such that the b_n are sections of $-nK_B$. Different types of singular fibers can then be engineered by making the coefficients b_n have appropriate vanishing degrees along a divisor $\zeta_0 = 0$ of the base.

This presentation can be rephrased in terms of toric geometry by constructing a fan Σ with v_i given by

$$v_x = \begin{pmatrix} -1 \\ 0 \\ 0 \end{pmatrix}\,,\; v_y = \begin{pmatrix} 0 \\ -1 \\ 0 \end{pmatrix}\,,\; v_w = \begin{pmatrix} 2 \\ 3 \\ 0 \end{pmatrix}\,,\; v_{\zeta_0} = \begin{pmatrix} 2 \\ 3 \\ 1 \end{pmatrix}\,. \tag{3.9}$$

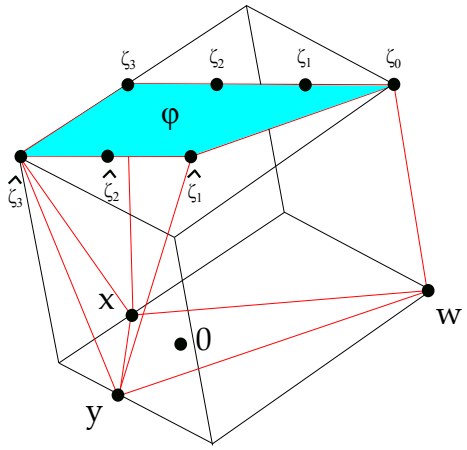

Figure 2: Toric top and fiber face φ (in blue) for and I_7 Kodaira singular fiber, with the cone generators corresponding to v_{ζ_i} and $v_{\hat{\zeta}_i}$. The coordinates are summarized in (3.9).

The fan Σ contains the following three-dimensional cones

$$\langle v_x, v_y, v_{\zeta_0}\rangle\,, \langle v_x, v_w, v_{\zeta_0}\rangle\,, \langle v_w, v_y, v_{\zeta_0}\rangle\,. \tag{3.10}$$

We may then capture the leading terms (in ζ_0) in (3.8) via (3.7) in terms of points on a Newton polyhedron Δ.

This presentation allows for a straightforward application of the techniques discussed above to find all crepant weighted blowups. If we perform a blowup associated with a refinement $\Sigma' \to \Sigma$, which introduces a single one-dimensional cone with generator v_E, the anticanonical class of T_Σ receives the contribution

$$\delta K = \left(a_E - \sum_i a_i\right) D_E\,. \tag{3.11}$$

This tells us that the above only is a crepant (partial) resolution of X if its class after the proper transform is $-K_{X_\Sigma} - \delta K$. In other words, the proper transform must allow us to 'divide out' the right power of the exceptional coordinate z_E to make $P(z_i)$ acquire the weight $(-a_E + \sum_i a_i)$ under the $\mathbb{C}^*$ action (3.4).

A weighted blowup sends $z_i \to z_i z_E^{a_1/a_E}$. In order for such a blowup to be crepant, (3.7) must be divided by $z_E^{(-a_E+\sum_i a_i)/a_E}$ under the proper transform. Using (3.4), any monomial in

(3.7) is then turned into

$$\begin{aligned} & z_E^{(a_E-\sum_i a_i)/a_E} \prod_i z_i^{\langle m_j,v_i\rangle+1} z_E^{\frac{1}{a_E}(a_i\langle m_j,v_i\rangle+a_i)} \\ =& z_E^{(a_E-\sum_i a_i)/a_E} z_E^{\langle m_j,v_E\rangle+\sum_i a_i/a_E} \prod_i z_i^{\langle m_j,v_i\rangle+1} \\ =& z_E^{\langle m_j,v_E\rangle+1} \prod_i z_i^{\langle m_j,v_i\rangle+1}, \end{aligned} \tag{3.12}$$

i.e. we simply need to use (3.7) for the new coordinate z_E as well. Note, however, that (3.12) is a holomorphic section if and only if

$$\langle m_j, v_E\rangle \geq -1 \qquad \text{for all} \quad m_j\,, \tag{3.13}$$

and hence only blowups related to the introduction of new generators v_E satisfying this relation can be crepant. For a given singularity[4] in (3.8), this will single out a finite number of crepant weighted blowups. After performing such a weighted blowup (cone refinement), the set m_j of monomials is not changed, i.e. at every step of a sequence of blowups we find the same condition (3.13) for the next step. We hence learn that we can only use weighted blowups originating from the set of v_E satisfying (3.13) in any step of a sequence of blowups.

The finite number of points above the v_x, v_y, v_w plane satisfying (3.13) form the tops [26, 33, 34] corresponding to various degenerate fibers in Tate models. An example is shown in figure 2.

Even though tops naturally appear in the study of toric hypersurfaces, they have a more general applicability. The above argument shows that given any elliptic Calabi-Yau manifold for which the fiber is given by a Weierstrass model, and a singularity is engineered via assigning vanishing orders, we may use the corresponding top (3.13) to find all weighted crepant blowups for which the fiber persists to be embedded as a hypersurface.

3.4 Triangulations of Tops and Fiber Faces

As discussed in the last section, weighted blowups are crepant if the exceptional divisors correspond to lattice points on the relevant top. However, performing resolutions through sequences of weighted blowups is inconvenient for two reasons: First of all, we may end up with the same resolution although we have performed two different sequences of weighted blowups, see the figure 17 and the related discussion for an example. Here, constructing the

[4]We are only interested in singularities which can be resolved by refining the cone spanned by v_x, v_y and v_{ζ_0}.

associated fan of the ambient space provides a convenient way of identifying (in)equivalent resolutions. As we already know that the rays of this fan will be sitting on the relevant top, each sequence of blowups will yield a triangulation of this top. Secondly, sequences of weighted blowups are not the most general resolutions which can be conveniently described by toric methods. In fact, any refinement[5] of a fan supplies us with a morphism which may be used to construct a resolution [29]. In the case of tops, the fan refinements we are looking for are those associated with triangulations and it turns out that not all triangulations can be obtained through a series of weighted blowups, an easy example is given in figure 18.

For these reasons, we can conveniently characterize different resolutions of elliptic singularities by considering different triangulations of the associated tops. Note that all of the corresponding models are described by the same hypersurface equation, which is essentially given by (3.7), and only the SR-ideal changes when we consider different triangulations. This will allow us to easily read off properties of the resolved geometries from triangulations.

Starting from a Weierstrass model, all singularities sit in the cone spanned by the rays v_x, v_y and v_{ζ_0} before resolution. Consequently, it is only this cone which is refined when performing a resolution. We can project the bouquet of cones sitting inside the cone $\langle v_x, v_y, v_{\zeta_0}\rangle$ after resolution to a plane resulting in a diagram showing which homogeneous coordinates are allowed to vanish simultaneously. We call this type of diagram a *fiber face* and it will prove very useful to conveniently read off which triangulation corresponds to which of the phases. An example is shown in figure 2.

3.5 Flops

For a toric variety, we may perform a flop if there are cones in the associated fan which can be re-triangulated as shown in the following figure, with four ray generators on a plane:

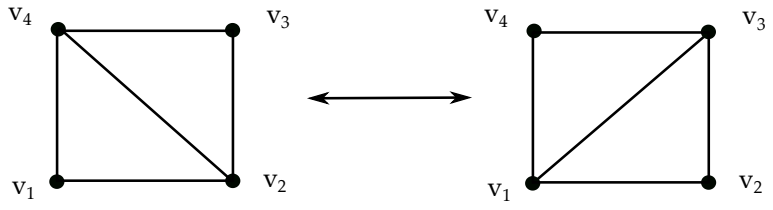

(3.14)

We may understand this flop as a two-step process in which we first take out the cone σ_{24} connecting v_2 and v_4, resulting in a singularity, and then introduce the cone σ_{13} connecting v_1 with v_3 to resolve. The cones σ_{24} and σ_{13} correspond to subvarieties of codimension two

[5]In contrast to elementary blowups, we have to make sure the resulting variety is still projective. The condition for projectivity says that the simplices need to be images of faces of a higher-dimensional polytope, see e.g. [29].

(intersection of two divisors) and each of these subvarieties have normal bundles in the Calabi-Yau $\mathcal{O}(-1) \oplus \mathcal{O}(-1)$.

For a Calabi-Yau hypersurface, or more generally complete intersection, embedded in a toric ambient space, performing a flop on the level of the ambient space induces a flop of the Calabi-Yau as well[6]. The class of flops of the Calabi-Yau which descend from such flops of the ambient space can be conveniently described in terms of re-triangulations of tops. However, there are also other flops for which this is not the case. This stems from the fact that not all rational curves descend from rational curves in the ambient space. Flop transitions involving such curves are much harder to determine, and will be of consideration in the following.

4 Fiber Faces and Box Graphs for $\mathfrak{su}(2k+1)$

We will now show that for elliptic fibrations with I_{2k+1} singular fibers, corresponding to a gauge algebra $\mathfrak{su}(2k+1)$ with anti-symmetric matter, the algebraic resolutions as well as triangulations of the top/fiber faces yield (strict) subclasses of box graphs, and that there is a precise correspondence between the triangulations and the properties of the phases. The starting point for the toric resolutions is the Tate resolution (i.e. the resolution of the Tate model), which proceeds via a specific algebraic sequence of blowups, to be discussed in the next subsection. We then show how algebraic resolutions have a simple characterization in terms of specific box graphs, whose anti-Dyck path is a concatenation of corners ⌟ and ⌜. The toric resolutions obtained by top triangulations are explained in section 4.3. Finally the main argument identifying these with a sub-class of box graphs is given in section 4.4.

4.1 Tate Resolution

The gauge algebras $\mathfrak{su}(2k+1)$ are realized in F-theory in terms of singular fibers in codimension one of Kodaira type I_{2k+1}. There are two matter loci of interest, corresponding to the fundamental representation of dimension $2k+1$ and the anti-symmetric $\Lambda^2 V$ of dimension $(2k+1)k$. The singular Tate form is [24, 25]

$$y^2 + b_1 xy + b_3 y\zeta_0^k = x^3 + b_2\zeta_0 x^2 + b_4 x\zeta_0^{k+1} + b_6\zeta_0^{2k+1}\,, \tag{4.1}$$

where $\zeta_0 = 0$ is the discriminant component for which the discriminant has vanishing order $\Delta = O(\zeta_0^{2k+1})$, and above which the singular I_{2k+1} fiber is located. The two matter

[6]Of course, this is only true if the relevant subvariety which is flopped in the ambient space also meets the embedded Calabi-Yau.

enhancements occur along the following loci

$$\begin{aligned} \Lambda^2 V: &\qquad b_1 = 0 \\ V: &\qquad P_V = b_2 b_3^2 - b_1 b_3 b_4 + b_1^2 b_6 = 0\,. \end{aligned} \tag{4.2}$$

Resolutions of this class of models were described in [22] using algebraic blowups:

$$\begin{aligned} (x, y, \zeta_i; \zeta_{i+1})\,, &\qquad i = 0, \cdots k-1 \\ (y, \zeta_i; \hat{\zeta}_i)\,, &\qquad i = 1, \cdots, k\,. \end{aligned} \tag{4.3}$$

Here the notation indicates that the singular locus $x = y = \zeta_i = 0$ is blown up with new exceptional section ζ_{i+1}. This can also be expressed in terms of the $\mathbb{C}^*$ scalings

x	y	ζ_i	ζ_{i+1}	$\hat{\zeta}_i$
1	1	1	-1	0
0	1	1	0	-1

(4.4)

The resolved Tate model (in codimension one, two, and for four-folds, three) is

$$\begin{aligned} T_{2k+1}: &\qquad y^2 B(\hat{\zeta})\hat{\zeta}_k + b_1 xy + b_3 y \zeta_0^k B(\zeta\hat{\zeta}) C(\zeta\hat{\zeta}) \\ &= x^3 B(\zeta) A(\zeta\hat{\zeta}) \zeta_k^k \hat{\zeta}_k^{k-1} + b_2 x^2 \zeta_0 B(\zeta)\zeta_k + b_4 x \zeta_0^{k+1} B(\zeta^2\hat{\zeta}) C(\zeta\hat{\zeta})\zeta_k + b_6 \zeta_0^{2k+1} B(\zeta^3\hat{\zeta}^2) C(\zeta^2\hat{\zeta}^2)\zeta_k\,. \end{aligned} \tag{4.5}$$

where

$$A(z) = \prod_{i=2}^{k-1} z_i^{i-1}\,, \qquad C(z) = \prod_{i=1}^{k-2} z_i^{k-(i+1)}\,, \qquad B(z) = \prod_{i=1}^{k-1} z_i\,. \tag{4.6}$$

The fibers above the codimension one locus are given by rational curves, and the associated exceptional divisors can be described in terms of the exceptional sections as follows:

Simple root	Section	Equation in Y_4
α_0	ζ_0	$0 = \left[\prod_{i=2}^{k} \hat{\zeta}_i\right]\left(y^2\hat{\zeta}_1 - x^3 A(\zeta)B(\zeta)\zeta_k^k \left[\prod_{i=2}^{k-1} \hat{\zeta}_i^{i-2}\right]\hat{\zeta}_k^{k-2}\right) + b_1 xy$
$\alpha_{1\cdots k-1}$	$\zeta_{1,\cdots,k-1}$	$0 = y^2 B(\hat{\zeta})\hat{\zeta}_k + b_1 xy$
α_k	ζ_k	$0 = yB(\hat{\zeta})\left(y\hat{\zeta}_k + b_3\zeta_0^k B(\zeta)C(\zeta\hat{\zeta})\right) + b_1 xy$
α_{k+1}	$\hat{\zeta}_k$	$0 = B(\zeta)\Big(b_3 y\zeta_0^k B(\hat{\zeta})C(\zeta\hat{\zeta}) - b_2 x^2\zeta_0\zeta_k - b_4 x\zeta_0^{k+1}B(\zeta\hat{\zeta})C(\zeta\hat{\zeta})\zeta_k$ $-b_6\zeta_0^{2k+1}B(\zeta^2\hat{\zeta}^2)C(\zeta^2\hat{\zeta}^2)\zeta_k\Big) + b_1 xy$
$\alpha_{k+2\cdots 2k-1}$	$\hat{\zeta}_{k-1,\cdots,2}$	$0 = B(\zeta)\zeta_k b_2 x^2\zeta_0 + b_1 xy$
α_{2k}	$\hat{\zeta}_1$	$0 = x^2 B(\zeta)\zeta_k\left(xA(\zeta\hat{\zeta})\zeta_k^{k-1}\hat{\zeta}_k^{k-1} + b_2\zeta_0\right) - b_1 xy$

(4.7)

Here, the projective relations of the resolution were already used and the exceptional divisors, or Cartan Divisors, can be identified with the simple roots of $\mathfrak{su}(2k+1)$

$$\begin{aligned} D_{\alpha_i} &= D_{\zeta_i} &&\text{for} \quad i = 0, \cdots, k \\ D_{\alpha_i} &= D_{\hat{\zeta}_{2k+1-i}} &&\text{for} \quad i = k+1, \cdots, 2k\,. \end{aligned} \tag{4.8}$$

We will now consider various alternative resolutions, which will be shown to correspond to a subclass of box graphs.

4.2 Algebraic Resolutions and Hypercubes

The first class of resolutions we will consider are algebraic resolutions, which were studied for $\mathfrak{su}(5)$ in [16, 17] and for general Tate models in [22]. The starting point is the codimension one resolved Tate model, i.e. (4.5) with $\hat{\zeta}_i = 1$. This has the form of a binomial form

$$y\hat{y} = \left(\prod_{i=1}^{k} \zeta_i\right) \; P\,, \tag{4.9}$$

where

$$\begin{aligned} \hat{y} &= y + b_1 x + b_3 \zeta_0^k B(\zeta) C(\zeta) \\ P &= x^3 A(\zeta) \zeta_k^{k-1} + b_2 x^2 \zeta_0 + b_4 x \zeta_0^{k+1} B(\zeta) C(\zeta) + b_6 \zeta_0^{2k+1} B(\zeta^2) C(\zeta^2)\,, \end{aligned} \tag{4.10}$$

with the projective relations, obtained from the big resolutions $(x, y, \zeta_i; \zeta_{i+1})$. As we are interested in the case of $b_1 = 0$, i.e. matter in the anti-symmetric representation, the only relevant small resolutions are between y and ζ_i. The set of small resolutions is then

$$\text{AlgRes}_\sigma : \qquad (y, \zeta_i; \hat{\zeta}_{\sigma(i)}), \qquad i = 1, \cdots, k, \qquad \text{for a fixed } \sigma \in S_k\,. \tag{4.11}$$

Note that not all of these give inequivalent resolutions.

We can prove the following statement: The algebraic resolutions (4.11) are exactly the box graphs, which have anti-Dyck paths that are concatenations of corners of the type

. (4.12)

The resulting paths automatically satisfy the diagonal condition. For $\mathfrak{su}(7)$ the algebraic resolutions, and corresponding paths, are shown in figure 3.

The network of flops between these algebraic resolutions for $\mathfrak{su}(2k+1)$ is a hypercube in k dimensions, which follows straight forwardly from the decomposition into corners (4.12): every anti-Dyck path, can be labelled by $(\pm 1, \cdots, \pm 1)$, representing the decomposition into the two corners represented by ± 1 in (4.12). These are exactly points on a k dimensional hypercube, so there are 2^k such phases/resolutions. A flop is a map $\lrcorner \leftrightarrow \ulcorner$, which in the hypercube corresponds to moving along one of the edges, which exchanges $+1 \leftrightarrow -1$.

For $\mathfrak{su}(7)$, the 3d cube is shown in red in figure 15, for $\mathfrak{su}(5)$, the flop diagram for algebraic resolutions of singular elliptic fibrations with **10** matter is a square [5].

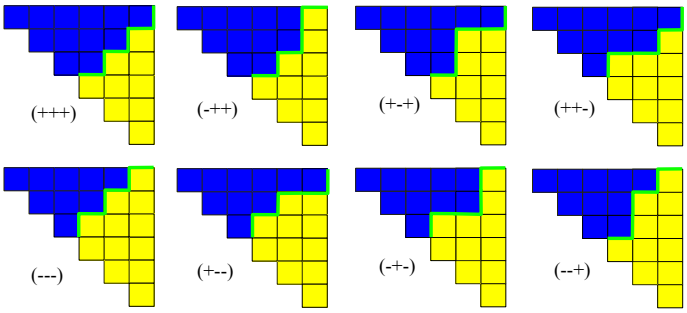

Figure 3: Example for $\mathfrak{su}(7)$: box graphs corresponding to algebraic resolutions, which are obtained as sequence of corners (4.12).

4.3 Fiber Face Triangulations

In this section we will identify the precise correspondence between toric hypersurface[7] resolutions, which are characterized by fiber face triangulations and a subclass of box graphs for $\mathfrak{su}(2k+1)$ with anti-symmetric matter.

4.3.1 Top and Fiber Face

We now discuss the resolutions of (4.1) using the toric techniques discussed in section 3. As a first step, let us record the defining data. If the generators of the rays corresponding to x, y, w, ζ_0 are fixed to be given by (3.9), the monomials in (4.1) correspond to the following lattice points

Monomial	y^2	$b_1 xy$	$b_3 y\zeta_0^k$	x^3	$b_2\zeta_0 x^2$	$b_4 x\zeta_0^{k+1}$	$b_6\zeta_0^{2k+1}$
Lattice Point	$\begin{pmatrix} -1 \\ 1 \\ 0 \end{pmatrix}$	$\begin{pmatrix} 0 \\ 0 \\ -1 \end{pmatrix}$	$\begin{pmatrix} 1 \\ 0 \\ k-3 \end{pmatrix}$	$\begin{pmatrix} -2 \\ 1 \\ 0 \end{pmatrix}$	$\begin{pmatrix} -1 \\ 1 \\ -1 \end{pmatrix}$	$\begin{pmatrix} 0 \\ 1 \\ k-3 \end{pmatrix}$	$\begin{pmatrix} 1 \\ 1 \\ 2k \end{pmatrix}$

(4.13)

Using (3.13), this means that any crepant resolution obtained by subdividing the fan must only use the rays

$$\begin{aligned} v_{\zeta_i} &= (2-i, 3-i, 1)\,, \qquad i = 1, \cdots, k \\ v_{\hat{\zeta}_i} &= (2-i, 2-i, 1)\,, \qquad i = 1, \cdots, k\,. \end{aligned} \tag{4.14}$$

An example of the top for $k = 3$ can be found in figure 2. In fact, we could have already obtained this from the fact that all of the blowups discussed in the previous sections are crepant. Translating these blowups into toric language shows that we need to subdivide the

[7]Here, of course, by hypersurface we always mean that the fiber is embedded as a hypersurface in a toric ambient space.

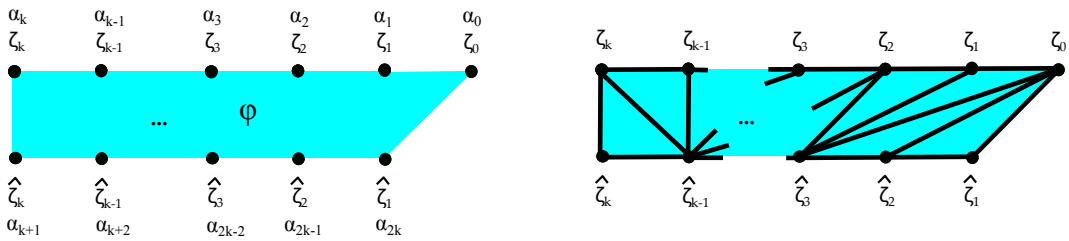
α_k α_{k-1} α_3 α_2 α_1 α_0
ζ_k ζ_{k-1} ζ_3 ζ_2 ζ_1 ζ_0
...
φ
$\hat{\zeta}_k$ $\hat{\zeta}_{k-1}$ $\hat{\zeta}_3$ $\hat{\zeta}_2$ $\hat{\zeta}_1$
α_{k+1} α_{k+2} α_{2k-2} α_{2k-1} α_{2k}
ζ_k ζ_{k-1} ζ_3 ζ_2 ζ_1 ζ_0
...
$\hat{\zeta}_k$ $\hat{\zeta}_{k-1}$ $\hat{\zeta}_3$ $\hat{\zeta}_2$ $\hat{\zeta}_1$

Figure 4: The picture on the left hand side shows the fiber face φ for $\mathfrak{su}(2k+1)$ with vertices ζ_i and $\hat{\zeta}_i$ defined in (4.14). The label α_i correspond to the simple roots that each node is associated with. On the right a sample triangulation of the fiber face is shown.

cone $\langle v_x, v_y, v_{\zeta_0}\rangle$ using the rays generated by (4.14). The algebraic resolutions discussed in section 4.2 are precisely those, in which we first subdivide using the coordinates ζ_i for $i = 1...k$ (in this order) and only then introduce the $\hat{\zeta}_i$ in an arbitrary order.

In general, we may of course subdivide the cone $\langle v_x, v_y, v_{\zeta_0}\rangle$ by introducing the points (4.14) in any order, or more generally, consider an arbitrary fine triangulation of the corresponding top. Any triangulation will contain the cones $\langle v_x, v_{\zeta_i}, v_{\zeta_{i+1}}\rangle$ $\langle v_x, v_{\zeta_k}, v_{\hat{\zeta}_k}\rangle$, $\langle v_y, v_{\hat{\zeta}_i}, v_{\hat{\zeta}_{i+1}}\rangle$ and $\langle v_y, v_{\hat{\zeta}_1}, v_{\zeta_0}\rangle$, so that a triangulation is specified by giving the simplices on the face containing the points (4.14). We can hence present a triangulation by drawing an image of what we call the fiber face, see figure 4. Given such a toric resolutions, one has to check projectivity. This is already guaranteed for triangulations related to sequences of weighted blowups as this necessarily preserves projectivity. In the general case, we can argue like this. A toric variety is projective if there is a piecewise linear and strongly convex support function on the cones of its fan. This is equivalent to the simplices of our triangulation being the images of faces of a polytope embedded in a higher-dimensional space. In the present case, this can easily be seen to be true: for any triangulation, one may distribute the ζ_i and $\hat{\zeta}_j$ along an arch such that all of the simplices become faces. In the present case any triangulation gives rise to a projective toric ambient space.

Summarizing the above discussion, sequences of weighted blowups are a subclass of resolutions as toric hypersurfaces which in turn can be constructed via triangulations. As shown in appendix A, there are $\binom{2k-1}{k}$ such triangulations. By construction, such resolutions will all lead to the same defining equation, (4.5), and only differ in the SR ideal, which can be read off from the triangulation.

Let us now discuss the structure of fiber components. At a generic point of the locus ζ_0, the fiber will split into $2k+1$ components, as the proper transform for any resolution is $\zeta_0 \to \zeta_0 \prod_i \zeta_i \hat{\zeta}_i$. We can hence identify the points in 4 with the Cartan divisors. Over codimension one in the base, two such divisors will only intersect if they are connected by a

one-simplex of the triangulation along an edge of the top (see e.g. [26,33]), i.e. we can identify

$$\begin{aligned} D_{\alpha_i} &= D_{\zeta_i} \qquad\qquad \text{for} \quad i = 0, \cdots, k \\ D_{\alpha_i} &= D_{\hat{\zeta}_{2k+1-i}} \qquad \text{for} \quad i = k+1, \cdots, 2k\,. \end{aligned} \tag{4.15}$$

Spelled out more explicitly, the expressions for the irreducible codimension-one fiber components are as in (4.7) and one may use this to check more explicitly that the identification (4.15) is sensible.

4.3.2 Flops

For two distinct triangulations which only differ by two simplices (and hence cones in the fan),

$$\begin{aligned} \varphi_1 \supset & \langle \zeta_k, \zeta_{k+1}, \hat{\zeta}_l \rangle\,, \langle \zeta_{k+1}, \zeta_l, \hat{\zeta}_{l+1} \rangle \\ \varphi_2 \supset & \langle \zeta_k, \zeta_{k+1}, \hat{\zeta}_{l+1} \rangle\,, \langle \zeta_k, \hat{\zeta}_l, \hat{\zeta}_{l+1} \rangle \end{aligned} \tag{4.16}$$

both fans can be seen as a subdivision of a fan containing the 'fused' cone

$$\varphi_{1\cup 2} \supset \langle \zeta_k, \zeta_{k+1}, \hat{\zeta}_l, \hat{\zeta}_{l+1} \rangle\,. \tag{4.17}$$

In other words, the fiber face contains four vertices which are positions as shown in (3.14). Correspondingly, the geometrical transition between the two phases determined by triangulations φ_1 and φ_2 is a flop, both at the level of the ambient space and the level of the embedded Calabi-Yau (4.5). It is not hard to see that all triangulations of the fiber face are linked by passing through a number of transitions of this type. Hence all phases realized by triangulations are connected via flop transitions.

4.3.3 Anti-Symmetric Representation

We now turn to the splitting of fiber components above $b_1 = 0$, corresponding to matter in the anti-symmetric $\Lambda^2\mathbf{2k+1}$ representation, where the fiber type enhances from I_{2k+1} to I^*_{2k-3}. This occurs over codimension two in the base, and thus, the 'connections' along the fiber face φ, i.e. the triangulation data, becomes relevant in characterizing the fibers. One-simplices connecting a divisor ζ_j with $\hat{\zeta}_l$ (for $j, l \neq k$) indicate that the two divisors intersect along a codimension two locus in the base. As such pairs are never neighbouring Cartan divisors, this can only happen if the two divisors share a common component, which means there is a component of multiplicity at least two over the corresponding locus. The one-simplices, which connect the ζ_i with $\hat{\zeta}_i$ hence gives us information relevant to the phase with respect to the antisymmetric representation. Let us discuss this in a bit more detail by analysing the behaviour of the different Cartan divisors over $b_1 = 0$ in turn, which will then enable us to identify the corresponding box graphs.

α_0: Over $b_1 = 0$, the number of irreducible components ζ_0 splits into depends on how many of the coordinates $\hat{\zeta}_i$, $i = 2..k$ are allowed to vanish simultaneously with ζ_0. In toric language, this means we have to count the number of one-simplices of the considered triangulation φ, which contain v_{ζ_0} and one of the $v_{\hat{\zeta}_i}$, $i = 2, \cdots, k$. Note that this number can be zero, depending on the triangulation. There is always at least one component over $\zeta_0 = \left(y^2\hat{\zeta}_1 - x^3 A(\zeta)B(\zeta)\zeta_k^k \left[\prod_{i=2}^{k-1} \hat{\zeta}_i^{i-2}\right] \hat{\zeta}_k^{k-2}\right) = 0$. As there is always a one-simplex connecting v_{ζ_0} with $v_{\hat{\zeta}_1}$, we can summarize the splitting rule of ζ_0 by saying that the number of components it splits into is equal to the number of one-simplices connecting v_{ζ_0} with any of the $v_{\hat{\zeta}}$.

$\alpha_{i\neq 0}$: Considering $\zeta_i = 0$ for $i = 1, \cdots, k-1$, the number of components over $b_1 = 0$ is determined by the number of factors of $B(\hat{\zeta})\hat{\zeta}_k = \prod_{j=1}^{k} \hat{\zeta}_i$ that ζ_i is allowed to vanish simultaneously with. Again, this directly translates into the number of one-simplices connecting v_{ζ_i} with any of the $v_{\hat{\zeta}_j}$. Note that any triangulation will at least contain one such one-simplex.

Continuing in this fashion, one may easily see that all of the splittings over $b_1 = 0$ may be elegantly summarized by the simple rule:

Theorem 4.1 *Each fiber component F_ℓ corresponds to a root α_ℓ and a homogeneous coordinate according to the table above. Let $Z = \{\zeta_i \,|\, i = 0, \cdots, k\}$ and $\hat{Z} = \{\hat{\zeta}_i \,|\, i = 1, \cdots, k\}$. Above $b_1 = 0$, the rational curve F_ℓ corresponding to the section $\zeta_i \in Z$ splits into n_ℓ components, where*

$$n_\ell = \#\textit{connections between } \zeta_i \textit{ and any element in } \hat{Z}. \tag{4.18}$$

Likewise, if F_ℓ corresponds to $\hat{\zeta}_i$, then the number of splitting components is the number of connections between $\hat{\zeta}_i$ and any element of Z.

Let us now see how many resolutions can be obtained in the way outlined above for $\mathfrak{su}(2k+1)$ with $\Lambda^2 V$. As any two such triangulations of the fiber face φ determine a different phase, this question is equivalent to determining the number of triangulations of φ. Using (A.2) derived in appendix A, we find that this number is given by

$$\#\text{Triangulations } = 2\binom{2k-1}{k}. \tag{4.19}$$

The factor of 2 arises as we get two phases from each triangulation by reordering the simple roots. Note that we can also easily reproduce the total number of fiber components (counted with multiplicities) over the $b_1 = 0$ locus. From the above discussion it follows that we simply

need to count the number of one-simplices connecting the two sides of the fiber face, as each gives rise to two components over $b_1 = 0$. For any triangulation, there are $2k$ such one-simplices, so that we find a total of $4k$ components which matches with the $(2k+2-4)\cdot 2+4 = 4k$ components expected for a fiber of type I^*_{2k-3}.

4.3.4 Fundamental Representation

Let us now discuss which fiber component splits over the matter curve carrying the fundamental representation, i.e. over $P = b_1^2 b_6 - b_2 b_3^2 + b_1 b_3 b_4 = 0$. Consider the fiber component corresponding to the root α_{k+1}. Over $b_1^2 b_6 - b_2 b_3^2 + b_1 b_3 b_4 = 0$, it splits into the two components

$$\begin{aligned} 0 &= b_1 x + b_3 B(\zeta\hat{\zeta}) C(\zeta\hat{\zeta}) \zeta_0^k \\ 0 &= b_1^2 y - b_1 b_2 x B(\zeta)\zeta_0\zeta_k + b_2 b_3 B(\zeta^2\hat{\zeta}) C(\zeta\hat{\zeta})\zeta_0^{k+1}\zeta_k - b_1 b_4 B(\zeta^2\hat{\zeta}) C(\zeta\hat{\zeta})\zeta_0^{k+1}\zeta_k \,. \end{aligned} \tag{4.20}$$

Note that this statement is completely independent of which triangulation we have choosen, so that we conclude that *all models* in which the fiber is realized as toric hypersurface are in the same phase with respect to the fundamental representation. Similarly, one easily convince oneself that all other fiber components stay irreducible over the matter curve related to the fundamental representation.

4.4 Coulomb Phases/Box Graphs for Triangulations of Tops

We now turn to the alternative description of the fiber face triangulations in terms of Coulomb phases, or equivalently box graphs. The fiber face triangulations correspond to a sub-class of box graphs which can be characterized as follows.

Theorem 4.2 *There is a one-to-one correspondence between fiber face triangulations (4.14) for an I_{2k+1} fiber in codimension one with enhancement to I^*_{2k-3} (or $\mathfrak{so}(4k+2)$) along the codimension one locus $b_1 = 0$, and the box graphs, which correspond to the following decorations of the representation graph of $\Lambda^2(\mathbf{2k+1})$.*

(a) The weights $L_i + L_j$ with $i \in [1,k]$ and $j \in [2,k+1]$ are assigned $+$ (i.e. the boxes are colored blue)

(b) The weights $L_i + L_j$ with $i \in [k+1, 2k-1]$ and $j \in [k+2, 2k]$ are assigned $-$ (i.e. the boxes are colored yellow)

(c) Any sign assignments in the remaining $k \times k$ square in the representation graph with weights $L_i + L_j$, $i \in [1,k]$ and $j \in [k+2, 2k+1]$, which obeys the flow rules then defines a consistent box graph, and corresponds to exactly one fiber face triangulation.

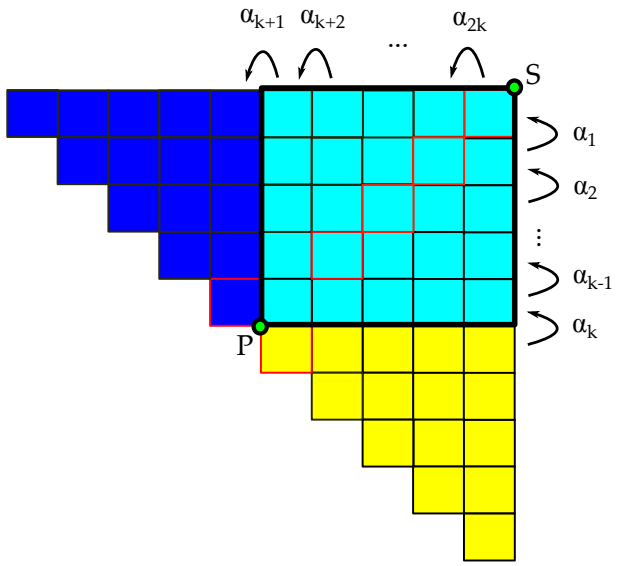

Figure 5: Box Graphs corresponding to fiber face triangulations. Blue/yellow are fixed +/− sign assignments, and each sign assignment/coloring of the turquois region (satisfying the consistency requirements, i.e. trace condition and flow rules for box graphs) corresponds to a triangulation of a fiber face.

Equivalently, the anti-Dyck paths starting at the point S and ending at P, as marked in figure 5, are one to one with toric fiber face triangulations.

We have shown the structure of the toric box graphs in figure 5, where the turquois colored region can be filled with any sign assignment which satisfies the flow rules. The + (blue) and - (yellow) colorings in the remaining triangles defined by (a) and (b) in the theorem, respectively, are fixed. Any sign changes in those regions will correspond to deviations from fiber face triangulations.

Before we prove the theorem, we recall how box graphs encode various properties of the codimension two fiber. A box graph for the $\Lambda^2 V$ representation determines a specific fiber by providing the extremal generators of the cone of effective curves along the codimension two locus $b_1 = 0$ in the Tate model, and their intersections. The central tool for that are the splitting rules, which specify how irreducible fiber components in codimension one split along the $b_1 = 0$ locus.

The **splitting rules** [35] applied to the current problem of $\Lambda^2 V$ for $\mathfrak{su}(2k+1)$ state: Given a box graph or equivalently anti-Dyck path, it can be decomposed into horizontal and vertical segments, separated by the corners of the path. We will denote these lines by H^i and V^i, when associated to horizontal or vertial lines in the box graph, which correspond to adding α_i. Recall that each vertical and horizontal wall in the box graph corresponds to a simple root

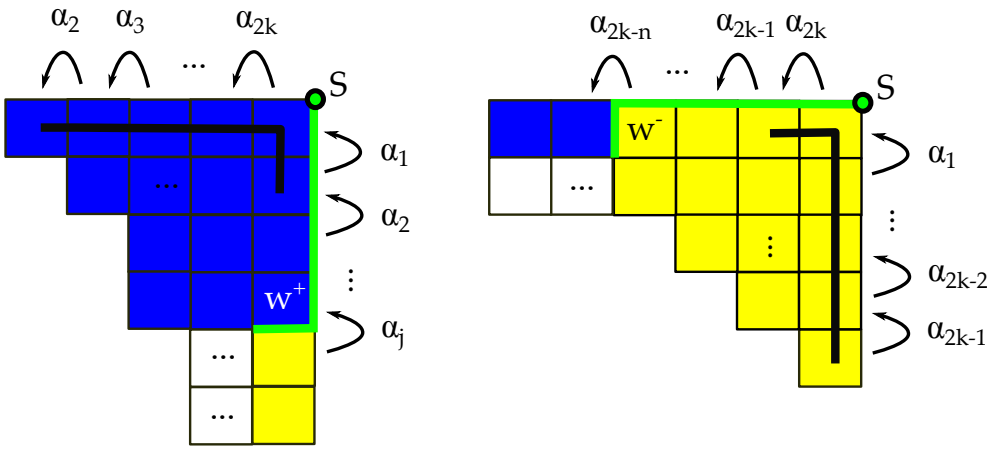

Figure 6: F_0 splitting rule: The F_0-hook is shown in bold-face black. Whenever a phase contains either of these, then F_0 splits.

$\alpha_i = L_i - L_{i+1}$, and whenever the anti-Dyck path crosses such a wall, the curve F_i labeled by the corresponding root splits along $b_1 = 0$.

- F_0 splitting:
  The affine node splits whenever the box graph contains the so-called "F_0-hook", i.e. a path through the box graph, which crosses all α_i-lines without changing the sign of the weights, I.e. whenever $F_0 = -\sum F_i$ 'fits' into the box graph. Equivalently, this can be characterized by the anti-Dyck path starting at the point S to move at least two boxes vertically down or at least two boxes horizontally to the left. In figure 6 we have shown such paths, with the black line indicating the F_0-hook, for which the splitting is

$$\begin{aligned} &\text{LHS figure 6: :} \quad F_0 \quad \to \quad C^+_{j,2k+1} + F_{j-1} + \cdots + F_2 + \tilde{F}_0\,, \qquad \tilde{F}_0 = C^-_{1,2} \\ &\text{RHS figure 6: :} \quad F_0 \quad \to \quad C^-_{1,n+1} + F_{2k-n-1} + \cdots + F_{2k-1} + \tilde{F}_0\,, \qquad \tilde{F}_0 = C^+_{2k-1,2k}\,. \end{aligned} \tag{4.21}$$

  Here $C^\pm$ are the curves corresponding to the extremal weight at the first corner of the anti-Dyck path that starts at S. $\tilde{F}_0$ is the affine node of the codimension two fiber, in particular it is not effective in the relative Mori cone.

- $F_{i\neq 0}$ splitting:
  For the splitting of the F_i consider first a horizontal segment of the anti-Dyck path, along the horizontal line H^j labeled by the simple root α_j, bounded by the vertical lines V^i and V^{i+n}, that correspond to adding α_i and α_{i+n}, as shown on the left of figure 7. Then the curve corresponding to α_j splits as follows

$$F_j \quad \to \quad C^-_{j-1,i+1} + F_{i+1} + \cdots + F_{i+n-1} + C^+_{j,i+n}\,. \tag{4.22}$$

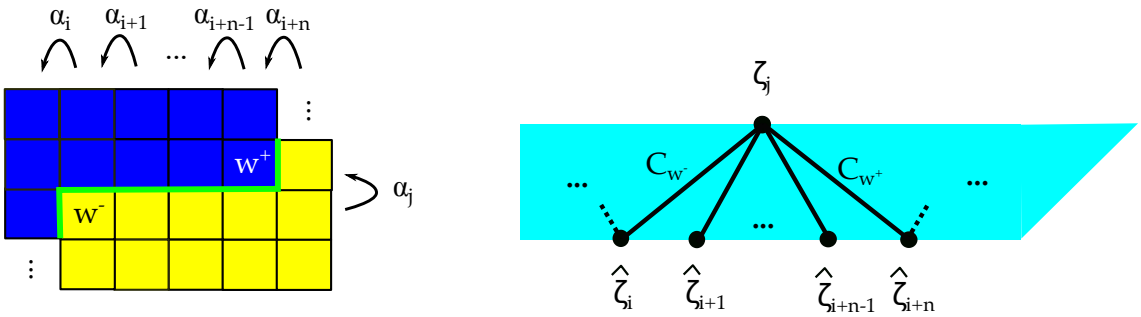

Figure 7: Splitting rule in terms of box graphs and corresponding 1-simplices in the toric fiber face triangulation.

Likewise a vertical segment of the anti-Dyck path between H^i and H^{i+j}, along V^n, results in the splitting of the curve associated to V^n into

$$F_n \quad \to \quad C^-_{i-1,n+1} + F_{i+1} + \cdots + F_{i+j-1} + C^+_{i+j,n}\,. \tag{4.23}$$

Proof of Theorem 4.2. The idea of the proof is to systematically derive the splitting from the box graphs, and to map this to a triangulation of the fiber face. This is done inductively, by starting at the point P of the box graphs, and determining the implied splitting from the anti-Dyck path. Roughly speaking one can think of each (horizontal or vertical) segment of the anti-Dyck path as specifying the 1-simplices that emanate from one of the vertices of the fiber face.

To prove the theorem, note first that any box graph defined by the rules (a)-(c) automatically is a consistent $\mathfrak{su}(2k+1)$ box graph, as the flow rules are satisfied and the signs $\epsilon(L_k + L_{k+1}) = +$ and $\epsilon(L_{k+1} + L_{k+2}) = -$ (which follow from (a) and (b)) guarantee, irrespective of the remaining signs in the region defined in (c), that the diagonal condition is satisfied.

A fiber face triangulation can be specified by the splitting of the fiber components along the codimension two locus $b_1 = 0$, which introduces 1-simplices (lines in the fiber face diagram), connecting the sections ζ_j with the sections $\hat{\zeta}_i$, which share common components. We now show that a given box graph of the type specified in the theorem yields a fine triangulation of the fiber face (or top) shown in figure 4 and defined in (4.14).

The box graph defines an anti-Dyck path, which starts at S and ends at P (which is the intersection of the vertical line V^{k+1} and horizontal line H^k). Starting at S, if the path proceeds horizontally/vertically, and turns at V^{2k} (H^1), F_0 does not split and there is no additional 1-simplex attached to the node ζ_0. Else, the path will turn at V^n or H^j, in which case the curve F_0 splits as in (4.21). This implies the 1-simplices shown in figure 8.

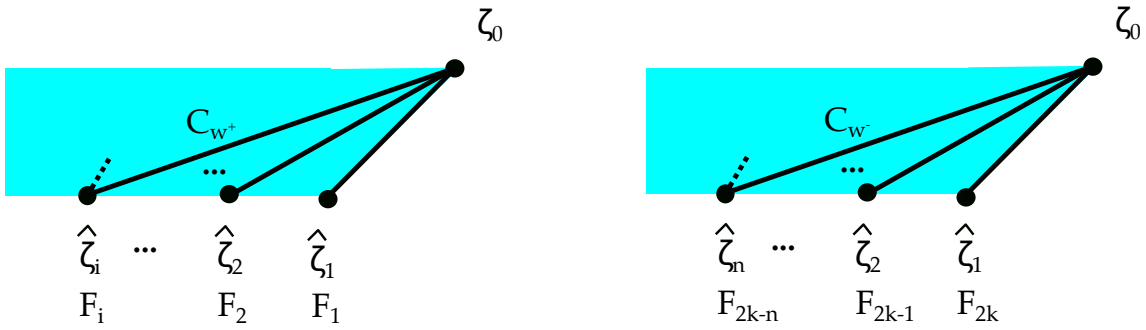

Figure 8: Splitting rule for F_0 as shown on the LHS/RHS of figure 6 implies the 1-simplices as shown here on the LHS/RHS. Depending on the initial splitting of F_0, which is given by $\zeta_0 = 0$, the assignement of simple roots α_i and associated curves F_i is determined in the diagram.

Furthermore, this initial segment (and the thereby resulting splitting of F_0) determines the identification between ζ_i, $\hat{\zeta}_i$ with the simple roots α_i:

- Dyck path segment starting at S is vertical: then for $i = 1, \cdots, k$

$$F_i \leftrightarrow \{\hat{\zeta}_i = 0\} \qquad F_{k+i} \leftrightarrow \{\zeta_{2k-i} = 0\}\,. \tag{4.24}$$

- Dyck path segment starting at S horizontal: then for $i = 1, \cdots, k$

$$F_i \leftrightarrow \{\zeta_i = 0\} \qquad F_{k+i} \leftrightarrow \{\hat{\zeta}_{2k-i} = 0\}\,. \tag{4.25}$$

The remaining 1-simplices for the triangulation are introduced by considering alternatingly the horizontal and vertical segments of the path. Consider first a horizontal segment along the line labeled by the simple root α_j[8], bounded by the vertical lines that correspond to adding α_i and α_{i+n}, as shown on the left hand side of figure 7. The anti-Dyck paths for fiber face triangulations are specified as starting at S and ending at the point P, therefore $j < i$. The splitting rules imply the following splitting along $b_1 = 0$

$$F_j \qquad \to \qquad C^-_{j-1,i+1} + F_{i+1} + \cdots + F_{i+n-1} + C^+_{j,i+n}\,. \tag{4.26}$$

Monotony of the anti-Dyck path implies that the path will not intersect the corresponding vertical lines again, and thus $F_{i+1}, \cdots, F_{i+n-1}$ are irreducible along $b_1 = 0$. The remaining components are the curves from the endpoints of this segment (which are the extremal generators of the cone of curves, and can be flopped). The curves F_i and F_{i+n} are also reducible,

[8]Without loss of generality, we consider the identification (4.25), which can be easily mapped to the identification of the sections with the roots should the splitting of F_0 imply the alternative identification (4.24).

with a component $C^-_{j-1,i+1}$ and $C^+_{j,i+n}$, with the remaining components being determined by the next (vertical segment) of the anti-Dyck path. The splitting (4.26) implies that there are 1-simplices in the fiber face triangulation, which connect ζ_j with each of the vertices $\hat{\zeta}_i, \cdots, \hat{\zeta}_{i+n}$. Furthermore irreducibility of $F_{i+1}, \cdots, F_{i+n-1}$ implies that these are the only 1-simplices that end on $\hat{\zeta}_{i+1}, \cdots, \hat{\zeta}_{i+n-1}$, which are shown in the corresponding triangulation on the RHS of figure 7. Monotony of the path implies that there is no crossing of 1-simplices, which would render the triangulation inconsistent.

Likewise a vertical segment, (4.23) implies the 1-simplices connecting $\hat{\zeta}_n$ with $\zeta_i, \cdots, \zeta_{i+j}$, where $\zeta_{i+1}, \cdots, \zeta_{i+j-1}$ are irreducible (which implies again due to the monotony of the path that these will only have 1-simplices connecting them to $\hat{\zeta}_n$), and ζ_i and ζ_{i+j} split along the adjacent horizontal lines as described above. Iterating this process results in a fine triangulation of the toric top.

Let us conclude with a simple counting argument of these box graphs. We can characterize these by monotonous staircase paths, starting at S and ending at P, which form a $k \times k$ grid. Note that the trace condition is already automatically satisfied for any sign assignment in the box graphs of the type in figure 5, and thus, the paths are only required to satisfy the flow rules, which translates into monotony. The number of such paths is

$$\#\text{Box graphs of the type in figure 5} = \binom{2k}{k}, \tag{4.27}$$

which agrees with the result in from the fiber face triangulations (4.19).

5 Secondary Fiber Faces and Complete Intersections

In the last section, we have shown how to construct all resolutions of $\mathfrak{su}(2k+1)$ fibrations for which the fiber is embedded as a toric hypersurface, and the starting point was a singular Weierstrass or Tate model. In terms of the box graphs this corresponded to anti-Dyck paths starting at S and ending at P in figure 5 (or P_1 in figure 12). In this section, we show how resolutions corresponding to paths ending at P_2 in figure 12 can be obtained from fibers embedded as complete intersections. They can be reached from the phases already considered via flops, and thus a straight-forward identification of their box graphs is possible. However, these generalized, so-called secondary fiber face triangulations, only realize a sub-class of the remaining phases. We discuss in section 6 how this decomposition of box graphs in terms of paths with varying endpoints can be emulated by embedding the fiber in an increasingly complex way.

5.1 Blowdowns and Elementary Flops

Phases that are beyond those corresponding to fiber face triangulations can be reached by chains of elementary flops, which map out of the class of box graphs in figure 5. Starting with the resolutions discussed in the last section, this will lead to geometries realized as complete intersections. Before discussing the general class of such resolutions, which will be done in section 5.2, we first consider elementary flops, obtained by blowdowns of toric divisors. We blow down a single coordinate from the ambient space and construct a new resolution, which cannot be realized as a hypersurface. The emerging structure is most easily seen by writing the resolved Tate model (4.5) in the two forms

$$T_{2k+1} \qquad \Leftrightarrow \qquad y\hat{y} = \prod_{i=1}^{k} \zeta_i \; P \tag{5.1}$$

and

$$T_{2k+1} \qquad \Leftrightarrow \qquad xW = \prod_{i=1}^{k-1} \hat{\zeta}_i \; S\,, \tag{5.2}$$

where we defined

$$\begin{aligned}
\hat{y} &= yB(\hat{\zeta})\hat{\zeta}_k + b_1 x + b_3 \zeta_0^k B(\zeta\hat{\zeta})C(\zeta\hat{\zeta}) \\
P &= x^3 A(\zeta\hat{\zeta})\zeta_k^{k-1}\hat{\zeta}_k^{k-1} + b_2 x^2 \zeta_0 + b_4 x \zeta_0^{k+1} B(\zeta\hat{\zeta})C(\zeta\hat{\zeta}) + b_6 \zeta_0^{2k+1} B(\zeta^2\hat{\zeta}^2)C(\zeta^2\hat{\zeta}^2) \\
W &= -b_1 y + x^2 B(\zeta)A(\zeta\hat{\zeta})\zeta_k^k\hat{\zeta}_k^{k-1} + b_2 x\zeta_0 B(\zeta)\zeta_k + b_4\zeta_0^{k+1}B(\zeta^2\hat{\zeta})C(\zeta\hat{\zeta})\zeta_k \\
S &= y^2\hat{\zeta}_k + b_3 y\zeta_0^k B(\zeta)C(\zeta\hat{\zeta}) - b_6\zeta_0^{2k+1}B(\zeta^3\hat{\zeta})C(\zeta^2\hat{\zeta}^2)\zeta_k\,.
\end{aligned} \tag{5.3}$$

The relevance of these forms is that they anticipate the conifold-like singularities, which may arise once one of the ζ_i or $\hat{\zeta}_i$ is blown down. Of course, as long as we use a fine triangulation of the top, we have resolved all singularities in codimensions one, two and three over the base and the factorized forms of (5.1) and (5.2) can never lead to a singularity. At a technical level, this happens because the coordinate y may never vanish simultaneously with any one of the coordinates ζ_i, and the coordinate x may never simultaneously vanish with any of the $\hat{\zeta}_i$ for $i = 1, \cdots, k-1$.

In toric language, a blowdown corresponds to a projection $\pi : \Sigma \to \Sigma'$ which maps every cone of Σ (in)to a cone in Σ'. In other words we can think of Σ' as arising by appropriately gluing together cones of Σ. Blowing down a coordinate z hence means that we have to glue cones such that the corresponding ray generated by v_z is not present in Σ'. Conversely, we may get back to Σ by blowing up Σ' via reintroducing v_z.

In the case at hand, we can only have a situation in which y can simultaneously vanish with ζ_i if we blow down $v_{\hat{\zeta}_i}$: as $v_{\hat{\zeta}_i} = v_{\zeta_i} + v_y$, it follows that $v_{\hat{\zeta}_i}$ sits in the middle between

v_{ζ_i} and v_y (a cone spanned by v_{ζ_i} and v_y contains $v_{\hat{\zeta}_i}$). Similarly, x can only simultaneously vanish with $\hat{\zeta}_i$ (for any $i = 1 \cdots k-1$) if we blow down ζ_{i+1} as $v_x + v_{\hat{\zeta}_i} = v_{\zeta_{i+1}}$.

We will use the notation $(z_1, \cdots, z_n | z_e)$ to indicate a blowdown which can be undone by a (weighted) blowup at $z_1 = \cdots = z_n = 0$ introducing the new coordinate z_e. We now discuss the various possible blowdowns and flops in turn.

5.1.1 Flops based on $(y, \zeta_1 | \hat{\zeta}_1)$ Blowdowns

Let us start by investigating blowdows of $\hat{\zeta}_1$. For such a blowdown to be possible, the triangulation of the fiber face in the vicinity of $v_{\hat{\zeta}_1}$ must be as shown in figure 9 (c). After the blowdown the four cones $\langle v_{\zeta_0}, v_y, v_{\hat{\zeta}_1}\rangle, \langle v_{\zeta_0}, v_{\zeta_1}, v_{\hat{\zeta}_1}\rangle, \langle v_{\hat{\zeta}_2}, v_y, v_{\hat{\zeta}_1}\rangle, \langle v_{\hat{\zeta}_2}, v_y, v_{\hat{\zeta}_1}\rangle$ are glued to $\langle v_{\zeta_0}, v_y, v_{\zeta_1}\rangle$ and $\langle v_{\zeta_1}, v_y, v_{\hat{\zeta}_2}\rangle$. Correspondingly, there is now a singularity at $y = \hat{y} = \zeta_1 = P = 0$ which implies $b_1 = 0$. We have hence blown down a fiber component over the $\Lambda^2 V$ matter curve.

We may perform a different resolution by blowing up along $y = P = 0$. To achieve this, we first introduce a new coordinate π and a new equation $\pi = P$. After this we may perform a small resolution $(y, \pi; \delta)$ resulting in

$$\begin{aligned} y\hat{y} &= \prod_{i=1}^{k} \zeta_i \; \pi \\ \delta\pi &= P\,. \end{aligned} \tag{5.4}$$

Let us now see how this has altered the splitting of fiber components over the $\Lambda^2 V$ matter curve at $b_1 = 0$. Note that in the phase before the blowdown, $D_{\alpha_{2k}}$ necessarily splits into two components, see figure 9 (c) and use the general rule formulated in theorem (4.1). After the resolution, the association of fiber components has changed, we now have

$$\begin{aligned} D_{\alpha_1}: &\qquad \zeta_1 = \delta y B(\hat{\zeta})\hat{\zeta}_k + b_1 x = 0 \\ D_{\alpha_{2k}}: &\qquad \zeta_1 = y = 0\,. \end{aligned} \tag{5.5}$$

Hence $D_{\alpha_{2k}}$ is now irreducible over any locus in the base. Over $b_1 = 0$, the fiber component D_{α_1} loses one component (the coordinate $\hat{\zeta}_1$ no longer appear in $B(\hat{\zeta})$ after the blowdown) but gains the two components at $y = 0$ and at $\delta = 0$. Hence we see that the total number of fiber components over $b_1 = 0$ stays constant: $D_{\alpha_{2k}}$ loses a component (so that it become irreducible over $b_1 = 0$) whereas D_{α_1} gains a component.

As such a flop is possible whenever the triangulation in the vicinity of ζ_1 is as shown in figure 9 (c), the number of which is given by

$$T_{k,k-1} = \binom{2k-3}{k-1}\,. \tag{5.6}$$

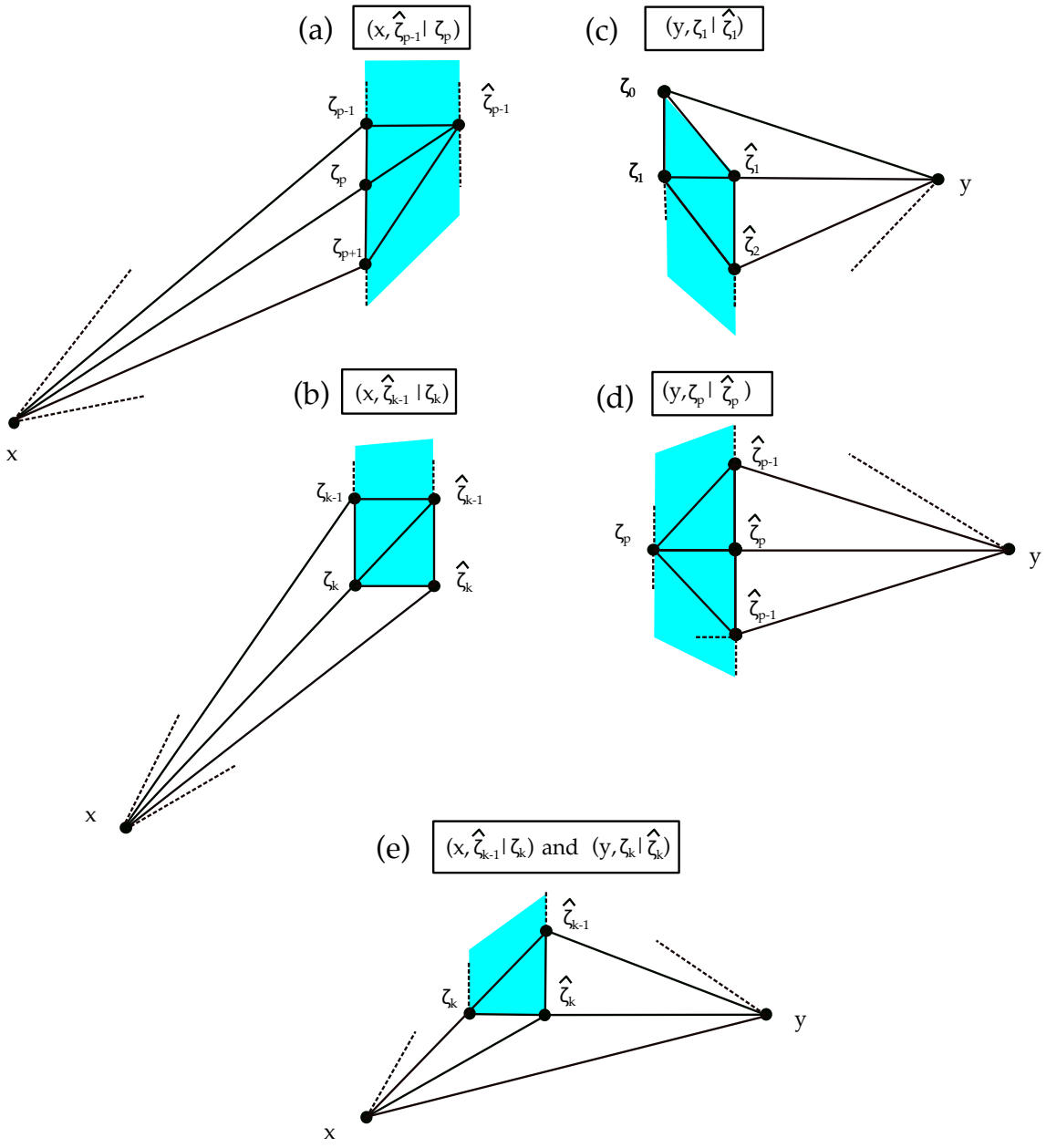

Figure 9: Toric triangulations for blowdowns and flops for I_n fibers. The notation is $(a, b|c)$, that we blow down c, which connects a and b.

5.1.2 The Blowdowns $(y, \zeta_p|\hat{\zeta}_p)$ for $0 < p < k$

Similarly, we may blow down any of the coordinates $\hat{\zeta}_p$ if we are in a phase with triangulation shown in figure 9 (d). Note that this means that the fiber component associated with $\hat{\zeta}_p$ stays irreducible over $b_1 = 0$. After the blowdown, we expect a singularity at $y = \hat{y} = \zeta_p = P = 0$. Again $y = \hat{y} = 0$ implies $b_1 = 0$, but now $P = \hat{\zeta}_p = 0$ implies $b_2 x^2 b \zeta_0 = 0$. As both x and ζ_0 cannot vanish at the same time as y and ζ_p, this implies $b_2 = 0$ and we conclude that this blowdown can never affect the splitting of fiber components over any of the matter curves. One also easily finds that performing a flop as in (5.4) does not alter the phase. It is not hard to see that the ambient space stays smooth after the blowdown as well.

5.1.3 Flops based on $(y, \zeta_k|\hat{\zeta}_k)$ Blowdowns

The blowdown $(y, \zeta_p|\hat{\zeta}_p)$, which can be performed when the triangulation is as shown in figure 9 (e), leads to a singularity at

$$y = \zeta_k = b_1 x + b_3 \zeta_0^k B(\zeta\hat{\zeta}) C(\zeta\hat{\zeta}) = b_2 x^2 \zeta_0 + b_4 x \zeta_0^{k+1} B(\zeta\hat{\zeta}) C(\zeta\hat{\zeta}) + b_6 \zeta_0^{2k+1} B(\zeta^2\hat{\zeta}^2) C(\zeta^2\hat{\zeta}^2) = 0\,. \tag{5.7}$$

These equations only have a common solution in the homogeneous coordinates $[x : B(\zeta\hat{\zeta})C(\zeta\hat{\zeta})]$ if we are over the matter curve of the fundamental representation, $P = b_2 b_3^2 - b_1 b_3 b_4 + b_1^2 b_6 = 0$. We hence expect the flop (5.4) to have no effect on the splitting over the $\Lambda^2 V$ matter, but only to affect the matter in the fundamental representation. After the blowdown, the divisor D_{ζ_k} becomes reducible and contains the fiber components

$$\begin{aligned} D_{\alpha_{k+1}}: &\quad \zeta_k = y = 0 \\ D_{\alpha_k}: &\quad \zeta_k = \hat{y} = 0\,. \end{aligned} \tag{5.8}$$

The fiber component corresponding to $D_{\alpha_{k+1}}$ stays irreducible over $P = 0$ in the flopped phase (5.4), whereas D_{α_k} splits into two components there.

There are

$$T_{k,k-1} = \binom{2k-3}{k-1} \tag{5.9}$$

cases, in which such a flop is possible.

5.1.4 Flops based on $(x, \hat{\zeta}_{k-1}|\zeta_k)$ Blowdowns

This blowdown is possible if the triangulation is as shown in figure 9 (b). Setting $x = \hat{\zeta}_{k-1} = W = S = 0$ implies $b_1 = 0$ and $y^2\hat{\zeta}_k + b_3 y \zeta_0^k B(\zeta) C(\zeta\hat{\zeta}) = 0$, so that there is now a singularity

at this locus. The relevant exceptional divisors after the flop become

$$\begin{aligned} D_{\alpha_k}: &\quad \hat{\zeta}_{k-1} = x = 0 \\ D_{\alpha_{k+2}}: &\quad \hat{\zeta}_{k-1} = W = 0\,. \end{aligned} \tag{5.10}$$

Note that now D_{α_k}, which was splitting into two components over $b_1 = 0$ has become irreducible. $D_{\alpha_{k+2}}$ has gained this component: over $b_1 = 0$, $W = \hat{\zeta}_{k-1} = S = 0$ implies that

$$\begin{aligned} b_2 \delta x \prod_{i=1}^{k-1} \zeta_i = 0 \\ y^2 \hat{\zeta}_k + b_3 y \zeta_0^k B(\zeta) C(\zeta\hat{\zeta}) = 0 \end{aligned} \tag{5.11}$$

While the component corresponding corresponding to a common solution of $\hat{\zeta}_{k-1}$ with ζ_k (this coordinate no longer exists) is lost, $D_{\alpha_{k+2}}$ has gained two more components at $x = 0$ and $\delta = 0$ over $b_1 = 0$. Such a flop can be performed in

$$T_{k,k-1} = \binom{2k-3}{k-1} \tag{5.12}$$

cases.

5.1.5 The Blowdowns $(x, \hat{\zeta}_{p-1}|\zeta_p)$ for $1 < p < k$

This type of blowdown is possible if the triangulation in the vicinity of ζ_p is as shown in figure 9 (a). When we blow down ζ_p, we expect a singularity over $x = \hat{\zeta}_{p-1} = W = S = 0$. Setting at $x = \hat{\zeta}_{p-1} = W = S = 0$ implies $b_1 = 0$ and $y^2\hat{\zeta}_k = 0$. As $v_{\hat{\zeta}_{p-1}}$ never shares a cone with $v_{\hat{\zeta}_k}$ and there is also never a common cone for v_x, v_y and $v_{\hat{\zeta}_{p-1}}$, we conclude that no singularity arises in this blowdown, and the ambient space stays smooth. Hence any blowdown $(x, \hat{\zeta}_{p-1}|\zeta_p)$, $1 < p < k$ can never lead to a flop/change of phase.

5.2 Complete Intersections and Secondary Fiber Faces

In this section, we generalize the construction above by blowing down more than just a single toric divisor. It turns out that blowing down all coordinates ζ_i for $i = 2, \cdots, k$ allows us to access a new class of resolutions, which go beyond the standard toric tops, and originate from box graphs which do not fall into the toric class figure 5. In the following, we will work with the form (5.2), i.e.

$$\begin{aligned} x\omega &= \prod_{i=1}^{k-1} \hat{\zeta}_i \; S \\ \omega &= -b_1 y + x^2 \zeta_1 A(\hat{\zeta}) \hat{\zeta}_k^{k-1} + b_2 x \zeta_0 \zeta_1 + b_4 \zeta_0^{k+1} \zeta_1^k B(\hat{\zeta}) C(\hat{\zeta})\,, \end{aligned} \tag{5.13}$$

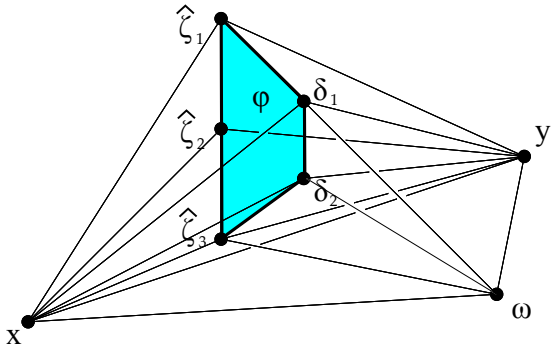

Figure 10: The secondary fiber face φ for the case of $\mathfrak{su}(7)$.

where ω is now a new coordinate. Torically, we enlarge the ambient space of the fan by one dimension, and associate the ray generated by $(0,0,0,1)$ with ω and lift all other cones of the fan. We give concrete description of this for $\mathfrak{su}(7)$ in (B.23). When all of the ζ_i (except ζ_0 and ζ_1) are blown-down, in particular, the corresponding cones are glued together, and then the resulting singularity is resolved by the set of resolutions

$$(\hat{\zeta}_i, \omega; \delta_i)\,, \qquad i = 1, \cdots, k-1\,, \tag{5.14}$$

we obtain

$$\begin{aligned} x\omega &= \left(\prod_{i=1}^{k-1} \hat{\zeta}_i\right) \left(y^2 \hat{\zeta}_k + b_3 y \zeta_0^k \zeta_1^{k-1} C(\hat{\zeta}\delta) - b_6 \zeta_0^{2k+1} \zeta_1^{2k-1} B(\hat{\zeta}\delta) C(\hat{\zeta}^2\delta^2)\right) \\ \left(\prod_{i=1}^{k-1} \delta_i\right) \omega &= -b_1 y + x^2 \zeta_1 A(\hat{\zeta}\delta) \hat{\zeta}_k^{k-1} + b_2 x \zeta_0 \zeta_1 + b_4 \zeta_0^{k+1} \zeta_1^k B(\hat{\zeta}\delta) C(\hat{\zeta}\delta)\,. \end{aligned} \tag{5.15}$$

Alternative resolutions of the form (5.13) are obtained by similar blowups, introducing the same coordinates δ_i, which however differ in the SR ideal, but not in the defining equation – much like in the case of the Tate resolution discussed earlier. As before, distinct resolutions are characterized in terms of triangulations of a face spanned by $\{\hat{\zeta}_1, \cdots, \hat{\zeta}_k, \delta_{k-1}, \cdots, \delta_1\}$, which we refer to as the *secondary fiber face* φ. This is shown in figure 10 for $\mathfrak{su}(7)$, including the remaining coordinates x, y, ω, as well as figure 11, which shows the secondary fiber face for $\mathfrak{su}(2k+1)$.

A triangulation ρ of the secondary fiber face φ gives rise to a fan with cones as summarized

in the following:

$$\begin{aligned}
&\langle x, y, \omega, \hat{\zeta}_k\rangle\,, \quad \langle x, \omega, \hat{\zeta}_k, \delta_{k-1}\rangle\,, \quad \langle y, \omega, \hat{\zeta}_k, \delta_{k-1}\rangle \\
&\langle \delta_i, \delta_{i+1}, \omega, x\rangle\,, \quad \langle \delta_i, \delta_{i+1}, \omega, y\rangle\,, \\
&\langle \rho, x\rangle\,, \quad \langle \rho, y\rangle\,, \\
&\langle \zeta_0, \zeta_1, x, \omega\rangle\,, \quad \langle \zeta_0, \zeta_1, \hat{\zeta}_1, \delta_1\rangle\,, \quad \langle \zeta_0, \zeta_1, \omega, \delta_1\rangle\,, \quad \langle \zeta_0, \hat{\zeta}_1, y, \delta_1\rangle \\
&\langle \zeta_0, \omega, y, \delta_1\rangle\,, \quad \langle \zeta_1, \hat{\zeta}_1, x, \delta_1\rangle\,, \quad \langle \zeta_1, x, \omega, \delta_1\rangle\,.
\end{aligned} \tag{5.16}$$

To determine the fibers, first consider codimension one, where the I_{2k+1} fiber components are identified with the sections as follows:

Simple root	Section	Equations in Y_4
α_0	ζ_0	$x\omega = y^2\prod_{i=1}^{k}\hat{\zeta}_i\,, \quad \omega\prod_{i=1}^{k-1}\delta_i = -b_1 y + x^2\zeta_1 A(\hat{\zeta}\delta)\hat{\zeta}_k^{k-1}$
α_1	ζ_1	$x\omega = y^2\prod_{i=1}^{k}\hat{\zeta}_i\,, \quad \omega\prod_{i=1}^{k-1}\delta_i = -b_1 y$
α_2	$\hat{\zeta}_1$	$x = 0\,, \quad \omega\prod_{i=1}^{k-1}\delta_i = -b_1 y$
$\alpha_{3,\cdots,k}$	$\hat{\zeta}_{2,\cdots,k-1}$	$x = 0\,, \quad \omega\prod_{i=1}^{k-1}\delta_i = -b_1 y$
α_{k+1}	$\hat{\zeta}_k$	$x\omega = \left(\prod_{i=1}^{k-1}\hat{\zeta}_i\right)\zeta_1^{k-1}\zeta_0^k C(\hat{\zeta}\delta)\left(b_3 y - b_6\zeta_0^{k+1}\zeta_1^k B(\hat{\zeta}\delta)C(\hat{\zeta}\delta)\right)$
		$\omega\prod_{i=1}^{k-1}\delta_i = -b_1 y + b_2 x\zeta_0\zeta_1 + b_4\zeta_0^{k+1}\zeta_1^k B(\hat{\zeta}\delta)C(\hat{\zeta}\delta)$
α_{k+2}	δ_{k-1}	$x\omega = \left(\prod_{i=1}^{k-1}\hat{\zeta}_i\right)\left(y^2\hat{\zeta}_k + b_3 y\zeta_0^k\zeta_1^{k-1}C(\hat{\zeta}\delta)\right)$
		$0 = -b_1 y + b_2 x\zeta_0\zeta_1$
$\alpha_{k+3,\cdots,2k-1}$	$\delta_{k-2,\cdots,2}$	$x\omega = y^2\prod_{i=1}^{k}\hat{\zeta}_i\,, \quad 0 = -b_1 y + b_2 x\zeta_0\zeta_1$
α_{2k}	δ_1	$x\omega = y^2\prod_{i=1}^{k}\hat{\zeta}_i\,, \quad 0 = -b_1 y + x^2\zeta_1 A(\hat{\zeta}\delta)\hat{\zeta}_k^{k-1} + b_2 x\zeta_0\zeta_1$

(5.17)

This identification in codimension one is independent of the triangulation of the fiber face. With this data, one may again work out how the various fiber components split over the $\Lambda^2 V$ matter curve. With the notation

$$X_\Delta(\zeta, \xi) = \#\text{ connections between } \zeta \text{ and } \xi \text{ in the triangulation}\,, \tag{5.18}$$

we can summarize the splitting rules along $b_1 = 0$ as follows:

Section	Equation along $b_1 = 0$	Number of components
ζ_0	(5.15)	1
ζ_1	$\delta_1 = 0$	1
$\hat{\zeta}_1$	$x = \prod_{i=1}^{k-1}\delta_i = 0$	$\sum_{i=1}^{k-1} X_\Delta(\hat{\zeta}_1, \delta_i)$
$\hat{\zeta}_j,\ j = 3, \cdots, k-1$	$x = \prod_{i=1}^{k-1}\delta_i = 0$	$\sum_{i=1}^{k-1} X_\Delta(\hat{\zeta}_j, \delta_i)$
$\hat{\zeta}_k$	(5.15)	$\sum_{i=1}^{k-1} X_\Delta(\hat{\zeta}_k, \delta_i)$
δ_{k-1}	$x = (y\hat{\zeta}_k + b_3\zeta_0^k\zeta_1^{k-1}C(\hat{\zeta}\delta))\prod_{i=1}^{k-1}\hat{\zeta}_i = 0$	$\sum_{i=1}^{k-1} X_\Delta(\delta_{k-1}, \hat{\zeta}_i)$
$\delta_j,\ j = 2, \cdots, k-2$	$x = \prod_{i=1}^{k}\hat{\zeta}_i = 0$	$\sum_{i=1}^{k} X_\Delta(\delta_j, \hat{\zeta}_i)$
δ_1	$x = \prod_{i=1}^{k}\hat{\zeta}_i = 0$	$\sum_{i=1}^{k} X_\Delta(\delta_1, \hat{\zeta}_i)$
	$\zeta_1 = x\omega - y^2\prod_{i=1}^{k}\hat{\zeta}_i = 0$	1
	$xA(\hat{\zeta}\delta)\hat{\zeta}_k^{k-1} + b_2\zeta_0 = x\omega - y^2\prod_{i=1}^{k}\hat{\zeta}_i = 0$	1

(5.19)

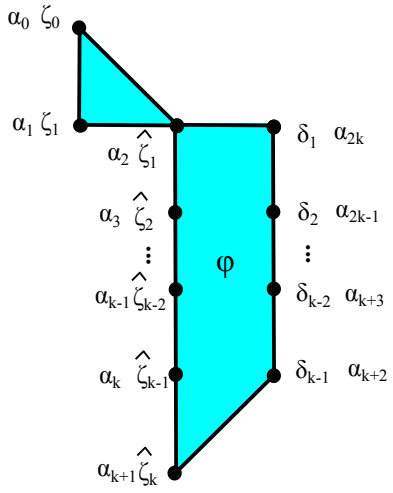

Figure 11: Secondary fiber face φ for the equations (5.15). Triangulations ρ of the fiber face φ correspond to resolutions that are characterized by the box graphs shown in figure 12. The labels indicate the simple root α_i, as well as the section $\hat{\zeta}$ or δ, associated to each node.

These splittings are in one-to-one correspondence with the splittings given in the box graphs of figure 12. The case of $\mathfrak{su}(7)$ with all the possible triangulations of φ is shown in figure 24. Note that the splitting rules follow a similar pattern to the fiber face triangulations. However, $\zeta_0, \zeta_1, \delta_1$ play a special role, which will also be clear from the splitting of $\alpha_0, \alpha_1, \alpha_{2k}$ in the associated box graphs, see figure 12.

5.3 Coulomb Phases/Box Graphs for Secondary Fiber Faces

The Coulomb phases associated to the secondary fiber face triangulations ρ_i, i.e. corresponding to the equations (5.15), are characterized in terms of box graphs, as shown in figure 12, where the blue/yellow colourings are fixed, and the only freedom in sign assignments (compatible with the flow rules) is in the turquoise box, bounded by the vertical lines V^{k+2} and V^{2k}, and horizontal lines H^2 and H^{k+1}. This implies in particular that F_{2k} is always reducible, and splits off one F_1. Furthermore, F_1 is irreducible. The sign assignment in the region bounded by these lines is only constrained by the flow rules, as the trace condition is already automatically satisfied ($\epsilon(L_{1,2k+1}) = -$ and $\epsilon(L_{2,2k}) = +$). Note also that we require at least one of the signs $\epsilon(L_{k+1,i})$, $i = k+2, \cdots, 2k+1$ to be positive, as otherwise the resulting box graphs already have a description in terms of standard toric top triangulations, which we already discussed. By the flow rules

$$\epsilon(L_{k+1,k+2}) = + \qquad \Rightarrow \qquad \epsilon(L_{i,k+2}) = +\,,\ i = 1, \cdots, k+1\,. \tag{5.20}$$

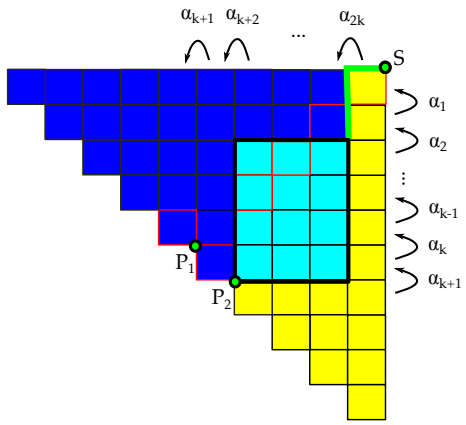

Figure 12: Box graphs realizing Coulomb phases, that correspond to the resolutions in (5.15). The fixed +/- sign assignments are shown in blue/yellow, whereas the possible triangulations are obtained by consistent sign assignments for the turquoise region, which satisfy the flow rules as well as the trace condition for $\mathfrak{su}(2k+1)$. The resulting geometries have a characterization in terms of triangulations ρ of the secondary fiber face φ in figure 11.

This implies that F_{k+1} is also reducible in codimension two. Following a similar reasoning to section 4.4, each sign assignment within this region results in a triangulation. This reduced set of box graphs is characterized in terms of the sign assignments as in figure 12. Again applying similar arguments to the ones in section 4.4, we can map these one-to-one to triangulations of the secondary fiber face φ. The number of such box graphs is again the number of monotonous lattice paths in a $(k-1) \times (k-2)$ grid, which is given by

$$\#\text{Box graphs as in figure 12} \;= \binom{2k-3}{k-1}. \tag{5.21}$$

This agrees with the number of triangulations of the secondary fiber face φ, as determined in appendix A

$$\#\text{Triangulations of } \varphi = T_{k,k-1} = \binom{2k-3}{k-1}. \tag{5.22}$$

Finally, it should be remarked that the toric hypersurface and complete intersection resolutions realize a subclass of the complete set of small resolutions. It is tantalizing to think that this process of blowdown and flop can be systematically generalized to cover all small resolutions that the box graphs predict. We will discuss this in appendix B in detail for the case of $\mathfrak{su}(7)$, which has (up to reordering) one additional phase, that does not fall into the category of resolutions discussed thus far.

6 Generalized Fiber Faces from Box Graph Layers

All of the phases discussed so far had a simple description matching that of the Coulomb phases/Box graphs, and furthermore all flops were realized by modifying the toric ambient space. This approach is convenient, as we can identify curves of the geometry as 2-dimensional cones, or equivalently 1-simplices on faces. Starting from box graphs, this gives a clear strategy for blow-downs or, more generally, flops. Unfortunately, at least in the present description, this structure does not persist to all Coulomb phases.

To conclude the general analysis of flops we now discuss how to realize the phases that go beyond the fiber face and secondary fiber face triangulations discussed so far. The next layer in the box graph description corresponds to changing signs outside the turquoise region in figure 12, and require flopping the curve $C^-_{k+2,k+3}$. The phase and fiber face triangulation, from which we start in order to access the next layer in the box graph is shown in figure 13. In this case only two of the curves corresponding to the roots α_i split over the matter curve $b_1 = 0$, they are

$$\begin{aligned} F_{2k} &\to C^+_{k+1,2k} + \sum_{i=1}^{k} F_i + C^-_{1,2k+1} \\ F_{k+1} &\to C^+_{k+1,2k} + \sum_{i=k+3}^{2k-1} F_i + C^-_{k+2,k+3}\,. \end{aligned} \tag{6.1}$$

Correspondingly, we can write the expression for $D_{\alpha_{k+1}}$ over $b_1 = 0$ (see (5.17)) as a matrix equation

$$M \begin{pmatrix} x \\ \prod_{i=1}^{k-2} \delta_i \end{pmatrix} = 0\,. \tag{6.2}$$

The components of $D_{\alpha_{k+1}}$ are now found by setting either $x = \delta_i = 0$ or $\det M = 0$. The first group of components are the ones shared with the D_{α_i}, for $i = k+3, \cdots, 2k$, and $C^-_{k+2,k+3}$ is identified as the component for which $\det M = 0$. Hence it cannot be identified as a stratum descending from the ambient space and we cannot flop it by re-triangulating the ambient space.

6.1 Flops to the next Layer

In order to flop the curve $C^-_{k+2,k+3}$ we take a more pedestrian approach in this section. For this consider the equations (5.15) in the patch where $\omega \neq 0$[9]. We can then solve the first equation for x and insert into the second equation, which yields again a hypersurface. To

[9]This assumption is without loss of generality, as none of the curves involved in the splittings have a component given by $\omega = 0$, as can be readily checked.

blow down the curve $C^-_{k+2,k+3}$, which is a component of $\hat{\zeta}_k = 0$ not shared with any of the δ_i, we note that a good coordinate on this curve is given by δ_{k-2}. More precisely, we can define the coordinates

$$\begin{aligned}
s_1 &= \hat{\zeta}_{k-1} \\
s_2 &= \delta_{k-2}\hat{\zeta}_{k-1} = \delta_{k-2}s_1 \\
s_3 &= -2A'(\delta\hat{\zeta})b_6B'(\delta\hat{\zeta})C'^3(\delta\hat{\zeta})\left(\prod_{i=1}^{k-2}\hat{\zeta}_i^2\right)s_1y\zeta_0^{3k+1}\zeta_1^{3k-1}\hat{\zeta}_k^{k-1}s_2^k \\
&\quad + A'(\delta\hat{\zeta})b_6^2B'^2(\delta\hat{\zeta})C'^4(\delta\hat{\zeta})\left(\prod_{i=1}^{k-2}\hat{\zeta}_i^2\right)\zeta_0^{4k+2}\zeta_1^{4k-1}\hat{\zeta}_k^{k-1}s_2^{k+2} \\
&\quad - aA'(\delta\hat{\zeta})b_6B'(\delta\hat{\zeta})C'^2(\delta\hat{\zeta})\left(\prod_{i=1}^{k-2}\hat{\zeta}_i^2\right)s_1^2y^2\zeta_0^{2k+1}\zeta_1^{2k}\hat{\zeta}_k^{k}s_2^{k-1} \\
&\quad - b_2b_6B'(\delta\hat{\zeta})C'^2(\delta\hat{\zeta})\left(\prod_{i=1}^{k-2}\hat{\zeta}_i\right)s_2^2\omega\zeta_0^{2k+2}\zeta_1^{2k} + b_4B'(\delta\hat{\zeta})C'(\delta\hat{\zeta})s_2\omega^2\zeta_0^{k+1}\zeta_1^k - \omega^3\delta_{k-2}\prod_{i=1}^{k-3}\delta_i \\
s_4 &= \delta_{k-2}s_3\,,
\end{aligned} \tag{6.3}$$

where we used the modified products (where all the δ_{k-2} and $\hat{\zeta}_{k-1}$ dependence is factored out)

$$A(\delta\hat{\zeta}) = s_2^{k-3}s_1A'(\delta\hat{\zeta})\,, \qquad B(\delta\hat{\zeta}) = s_2B'(\delta\hat{\zeta})\,, \qquad C(\delta\hat{\zeta}) = \delta_{k-2}C'(\delta\hat{\zeta})\,. \tag{6.4}$$

The hypersurface equation can then be written in the following way

$$\begin{aligned}
s_4 = &- b_1y\omega^2 + A'(\delta\hat{\zeta})C'^2(\delta\hat{\zeta})b_3^2\left(\prod_{i=1}^{k-2}\hat{\zeta}_i\right)s_1y^2\zeta_0^{2k}\zeta_1^{2k-1}\hat{\zeta}_k^{k-1}s_2^{k-1} \\
&+ 2b_3A'(\delta\hat{\zeta})C'(\delta\hat{\zeta})\left(\prod_{i=1}^{k-2}\hat{\zeta}_i^2\right)s_2^2y^3\zeta_0^k\zeta_1^k\hat{\zeta}_k^k s_2^{k-2} + A'(\delta\hat{\zeta})\left(\prod_{i=1}^{k-2}\hat{\zeta}_i^2\right)\zeta_1s_1^3y^4\hat{\zeta}_k^{k+1}s_2^{k-3} \\
&+ b_2b_3C'(\delta\hat{\zeta})\left(\prod_{i=1}^{k-2}\hat{\zeta}_i\right)s_2y\omega\zeta_0^{k+1}\zeta_1^k + b_2\zeta_0\zeta_1\left(\prod_{i=1}^{k-2}\hat{\zeta}_i\right)\hat{\zeta}_ks_1y^2\omega\,,
\end{aligned} \tag{6.5}$$

with the additional constraint that the new coordinates s_i need to satisfy the conifold equation:

$$s_1s_4 = s_2s_3\,. \tag{6.6}$$

We can then blow down the curve $C^-_{k+2,k+3}$ and blow up by e.g. introducing a new $\mathbb{P}^1$ with projective coordinates $[\xi_1, \xi_2]$ satisfying

$$s_1\xi_1 = \xi_2s_2\,, \qquad s_3\xi_1 = \xi_2s_4\,. \tag{6.7}$$

The fiber components F_i associated to the roots α_i, that are affected by this flop, split above the codimension two locus $b_1 = 0$ as follows:

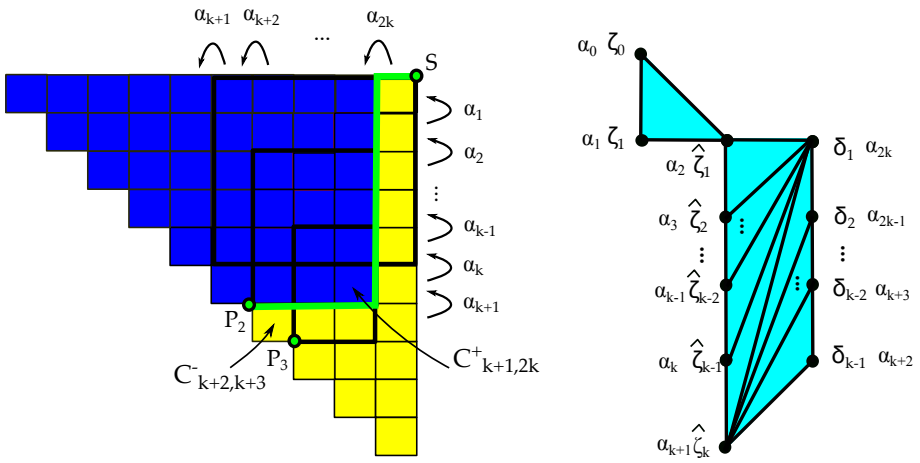

Figure 13: Box Graph and corresponding secondary fiber face triangulation, from which the next layer in the box graph can be accessed by flopping the curve $C^-_{k+2,k+3}$.

- F_{2k}: this is given by $\delta_1 = 0$, which has $k+2$ components after the flop
- F_{k+1}: this is $\hat{\zeta}_k = 0$, which looses one component after the flop, and splits into $k-2$ components
- F_{k+3}: this is given by $\delta_{k-2} = 0$, which in the new coordinates corresponds to $s_2 = s_4 = 0$, i.e. $\xi_2 = 0$ has now two components along $b_1 = 0$.

This is precisely the splitting that is expected from the box graph analysis after flopping the curve $C^-_{k+2,k+3}$. With this flop we have accessed the next 'layer' in the box graph, namely, the class of resolutions, which correspond to anti-Dyck paths ending at P_3 in figure 13.

6.2 Conjecture on Layer Structure

The analysis of the last section lends itself to a conjecture about how to construct the remaining phases. As we have seen in section 4, all phases for which the fiber is embedded as a toric hypersurface nicely organize themselves as anti-Dyck paths inside a square of the box graph, ending at P_1 in figure 14. In section 5 we gained access to another layer of curves by blowing down all of the coordinates ζ_i for $i = 2, \cdots, k$. The crucial point was that the elliptic fiber can be in turn described in the alternative factored form (5.2). This factorization makes manifest, after blowing down appropriate coordinates, the existence of conifold singularities, which can be used to pass to an alternative resolution. These have a characterization in terms of the triangulation of secondary fiber faces. We have shown that these are precisely the flops, which in the box graph language correspond to the phases for which the anti-Dyck path ends at P_2 in figure 14.

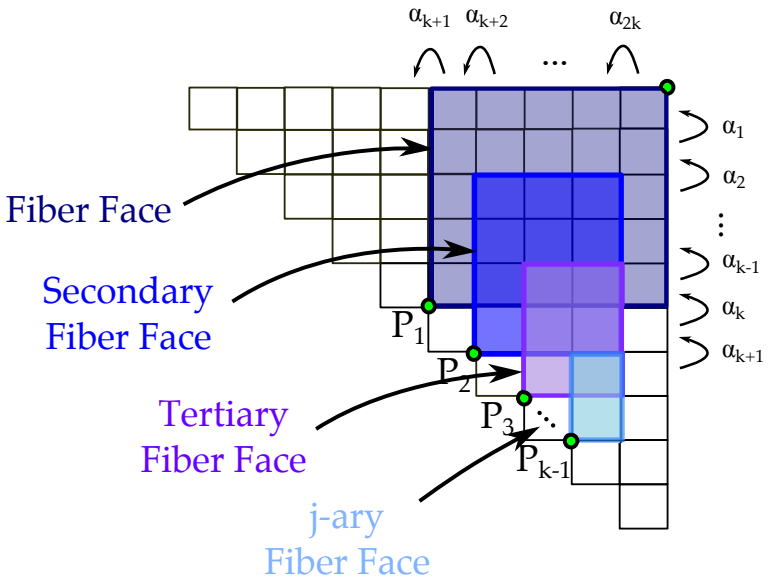

Figure 14: The layer structure of fiber faces within the box graphs for the anti-symmetric representation of $\mathfrak{su}(2k+1)$.

A completely analogous structure becomes apparent in (6.3). To achieve the flop of the curve $C^{-}_{k+2,k+3}$, we have essentially factored out δ_{k-2} from the terms contained in s_3 in (6.3). However, note that s_3 contains a factor of $\prod_{i=1}^{k-3}\delta_i$ as well. It is hence possible to introduce a similar birational map to the one defined in (6.3) by employing any of the coordinates δ_i for $i = 1 \cdots k-3$. Correspondingly, after blowdown, we expect there to be conifold singularities in (6.6), whereby we reach the set of phases for which the anti-Dyck paths end at P_3 of figure 14. Concretely, this will require all of the blowdowns associated with the δ_i for $i = 1 \cdots k-2$ at once, followed by the alternative small resolutions. This is expected to introduce $k-2$ new coordinates, forming a fiber face corresponding to P_3.

We conjecture that this structure prevails for *all* of the anti-Dyck paths, ending on the points P_i, i.e. there is a fiber face which is a strip with sides of length $k-i+2$ and $k-i+1$ associated to each class of paths, which end at one of the points P_i such that triangulations of the fiber face are in one-to-one correspondence with anti-Dyck paths ending at P_i of the box graph:

$$\text{Anti-Dyck Paths Ending at } P_j \quad \overset{1:1}{\longleftrightarrow} \quad j\text{-ary Fiber Face Triangulation} \tag{6.8}$$

It is not hard to see that a generalization of the splitting rules over $b_1 = 0$ observed in sections 4 and 5 perfectly match the behaviour of the fiber components predicted by the associated box graphs.

7 Discussion and Outlook

In this paper we studied the correspondence between resolutions of singular elliptic fibrations and box graphs (or equivalently, Coulomb phases of 3d supersymmetric gauge theories). We have proven the equivalence between a subclass of box graphs and a specific class of resolutions of the elliptic fibration. Each box graph has a unique identification with so-called anti-Dyck paths, and we showed that each resolution type is characterized in terms of paths ending at one fixed point on the diagonal. Moreover, we determined the network of flop transitions and showed the equivalence to the flops predicted by the box graphs.

More precisely, we have proven a one-to-one correspondence between resolutions obtained by toric methods (of triangulating the fiber face) and a class of box graphs. These have a unique characterization as anti-Dyck paths all ending in one fixed point on the diagonal (in this case, they end at the point P_1 in figure 14). Furthermore, we have shown that there is a secondary fiber face, which corresponds to another subclass of box graphs, characterized in terms of anti-Dyck paths ending at the point P_2 in figure 14. For these two classes we have shown in sections 4 and 5 that the triangulation of the fiber faces and box graph phases are in complete agreement.

Beyond these, we do not at present know how the class of resolutions has to be extended in order to account for the phases that are given in terms of box graphs. From our analysis, starting with the tops and then passing on to the secondary fiber faces, it seems rather suggestive that the box graphs can be somewhat "foliated" by generalized fiber face diagrams and their triangulations, as shown in figure 14. In other words, we expect each class of anti-Dyck paths with a fixed endpoint on the diagonal to give rise to a specific class of resolutions, as shown in figure 14.

As already observed in the companion paper [6] for $\mathfrak{su}(5)$, the resolutions cease to be of simple hypersurface or complete intersection type, and require for instance determinantal blowups. One direction to extend this would be to develop the connection to matrix factorization and resolutions as discussed in [36] as well as the more recent developments in [37, 38] addressing alternative ways of studying F-theory on singular spaces, or their deformations. Additionally, it would be interesting to extend our analysis to (combinations of) different matter representation and gauge algebras, such as the ones considered in [4].

Perhaps most thought-provokingly, one could anticipate to define a geometric structure starting from the box graphs, which is constructed from the data of the extremal generators and the knowledge of the splitting of rational curves in the fibers from codimension one to two. We leave these intriguing questions for future work.

Our results are also amenable to applications in mirror symmetry. In string theory, the Kähler moduli space of a Calabi-Yau variety is not confined to a single Kähler cone. In fact, it is natural to consider the union of all Kähler cones, that are related by flop transitions [39,40]. From this point of view, the box graphs yield the structure of the so-called enlarged Kähler cone for the Kähler moduli, which control the volumes of the fiber components (whilst keeping the Kähler moduli of the base fixed). Our results indicate that different phases of the same Calabi-Yau can have very different geometric realizations. The resolved elliptic fibers can for instance be embedded as hypersurfaces, complete intersections or more general algebraic varieties, which would in turn also change the geometric realization of the whole Calabi-Yau manifold in question.

Acknowledgements

We thank Philip Candelas, Xenia de la Ossa, Craig Lawrie, Dave Morrison and Jenny Wong for discussions on related matters. We thank the Aspen Center for Physics and the Galileo Galilei Institute in Florence for hospitality during the completion of this work. The research of APB was supported by the STFC grant ST/L000474/1 and the EPSCR grant EP/J010790/1. The work of SSN is supported in part by STFC grant ST/J002798/1. This work was in part performed at the Aspen Center for Physics, which is supported by National Science Foundation grant PHY-1066293. We furthermore thank the Aspen Asie fortune cookies for inspiration during the completion of this work.

A Number of Triangulations of a Strip

In this appendix, we derive an expression for the number of fine triangulations of the point configuration

$$P_{n,m} = \{(k,0)|[k = 1 \cdots n]\,, \quad (l,1)|[l = 1 \cdots m]\}\,, \tag{A.1}$$

i.e. we want to triangulate a strip which has n points on one side and m points on the other.

Let us denote the number of fine triangulations of $P_{m,n}$ by $T_{m,n}$. We now claim that

$$T_{n,m} = \binom{n+m-2}{n-1}\,, \tag{A.2}$$

which we are going to prove by induction. Note that this expression is symmetric under the exchange of $n \leftrightarrow m$. The first few terms are easy to check: by inspection one finds that e.g. $T_{1,m} = 1$, $T_{2,2} = 2$.

To proceed, we decompose the triangulations of $P_{n+1,m}$ in the following way. Let us single out the first point on the n-plane, i.e. $(1,0)$. It will necessarily have a 1-simplex connecting it to one of the points on the m-plane. Let us now assume the while it shares a 1-simplex with the point $(k_0,1)$, there is no point $(k,1)$ for $k > k_0$ with this property. Note that k_0 can be 1, in which case $(1,0)$ only meets $(1,1)$ along the boundary of the polytope spanned by the $P_{n,m}$. The crucial observation is now that for any fixed k_0, the triangulation "to the left" of the connecting one-simplex is uniquely fixed, whereas there are still $T_{n,m+1-k_0}$ ways to triangulations the part "to the right". Hence we have the recursion relation

$$T_{n+1,m} = \sum_{k_0=1}^{m} T_{n,m+1-k_0}\,. \tag{A.3}$$

To perform the induction step, we assume that the above holds for all $\hat{n} \leq n$ and $\hat{m} \leq m$ and wish to show that this implies that $T_{n+1,m}$ also satisfies (A.2). This is seen by writing

$$\begin{aligned} T_{n+1,m} &= \sum_{k_0=1}^{m} T_{n,m+1-k_0} \\ &= \sum_{k_0=1}^{m} \binom{n+m-k_0-1}{n-1} \\ &= \sum_{k=0}^{m-1} \binom{n-1+k}{n-1} \\ &= \binom{(n+1)+m-2}{m-1}\,. \end{aligned}$$

We have used that

$$\sum_{x=0}^{b} \binom{a+x}{a} = \binom{a+b+1}{b}\,. \tag{A.4}$$

Due to the symmetry between n and m this is sufficient to establish (A.2) for all n, m.

B Fibers and Phases for $\mathfrak{su}(7)$

As a concrete example, we consider phases of the $\mathfrak{su}(7)$ theory with anti-symmetric representation and construct all the phases geometrically. In $\mathfrak{su}(5)$ some features are less transparent due to the small rank, and the general structure becomes apparent only in the case of $\mathfrak{su}(7)$. The Tate form for an I_7 Kodaira fiber is

$$y^2 + b_1 xy + b_3 \zeta_0^3 y = x^3 + b_2 \zeta_0 x^2 + b_4 \zeta_0^4 x + b_6 \zeta_0^7\,. \tag{B.1}$$

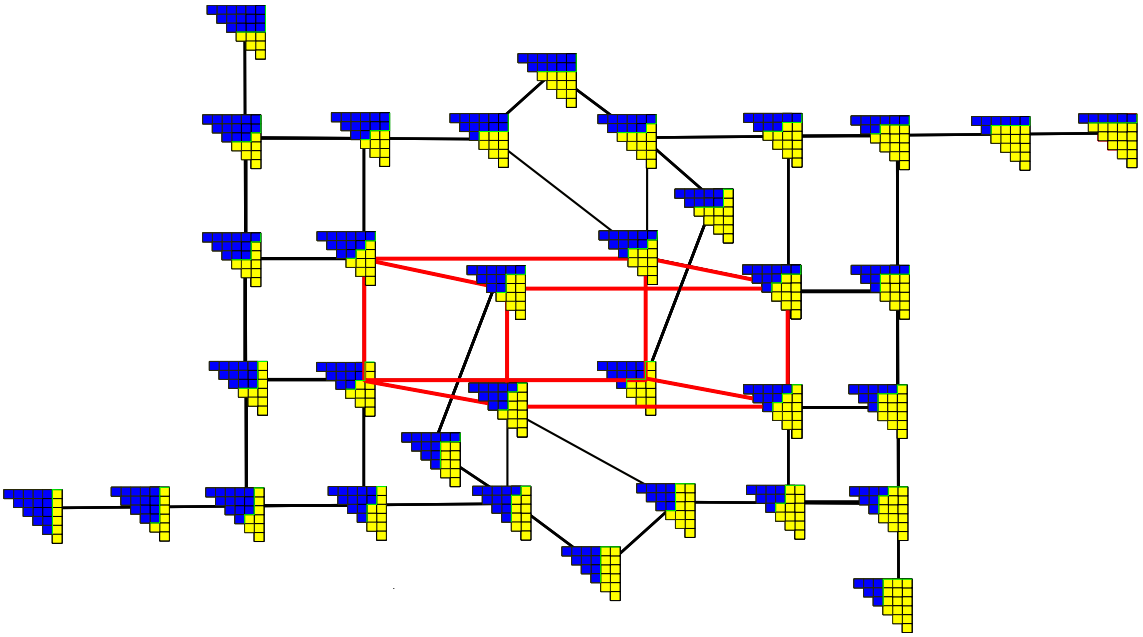

Figure 15: Box graphs for $\mathfrak{su}(7)$ with **21** matter, with lines connecting the box graphs corresponding to flop transitions. The cube shown with red connections corresponds to the standard algebraic resolutions discussed in more detail in section 4.2. The green lines, separating the blue/yellow (+/-) boxes correspond to the anti-Dyck paths. The geometric counterpart is shown in figure 16, where the geometric realization of these resolutions are shown.

Using the Weyl group quotient and trace condition, or equivalently the Box Graphs, one can determine the complete network of phases for $\mathfrak{su}(7)$ with $\mathbf{21} = \Lambda^2\mathbf{7}$. The codimension two locus, where this matter is localized in the Tate model is $\zeta_0 = b_1 = 0$.

B.1 Box Graphs

As shown in [4], there are 34 box graphs for $\mathfrak{su}(7)$ with $\Lambda^2\mathbf{7}$ with weights

$$w_{i,j} = L_i + L_j, \qquad i < j\,. \tag{B.2}$$

The signs have to satisfy the flow rules, i.e. + (blue) signs flow from right to left and below to above, and the oppositve for − signs (yellow). We will denote $w^{\pm}_{i,j} = \pm w_{i,j}$. For $SU(n)$ the tracelessness condition implies that there is a diagonal condition that needs to be satisfied. Alternatively, the resolution/phase can be characterized by the path that separates the weights that have a positive sign from those with a negative one. This anti-Dyck path has to cross the diagonal at least once, in order to ensure that the diagonal condition is satisfied. Flop transitions in box graphs are single box sign changes, which do not violate the flow rules and

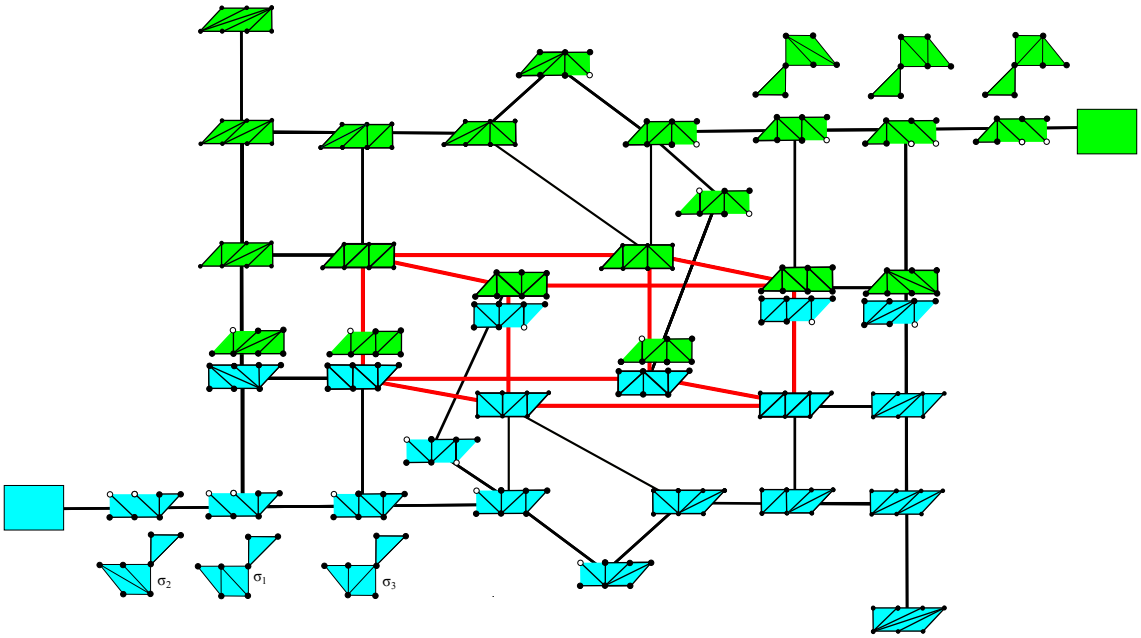

Figure 16: Resolution flop network for $\mathfrak{su}(7)$ with matter in the $\Lambda^2\mathbf{7}$ representation. This diagram is the geometric counterpart to the flop diagram for the box graphs in figure 15. The turquoise/green differ by reversing the orientation of the assignment between vertices and the fiber face and simple roots. Each diagram corresponds to a triangulation of either the toric top, or a blowdown of this, indicated by the white nodes. In particular the diagrams with multiple nodes blown-down have an alternative description in terms of triangulations of the secondary fiber face φ, see figure 24. Finally, the two empty squares correspond to box graphs, which do not seem to have a straight-forward toric description, however we will determine the corresponding resolution in section B.3.5.

diagonal condition. The resulting network of flop transitions is shown in figure 15 for $\mathfrak{su}(7)$ with the $\Lambda^2\mathbf{7}$ representation.

B.2 Fiber Faces and Weighted Blowups

B.2.1 Resolution

It is clear from the general analysis of [22] that for an I_7 fiber, three successive big resolutions resolve the geometry in codimension one:

$$y\left(y + b_1 x + b_3 \zeta_0^3 \zeta_1^2 \zeta_2\right) = \zeta_1 \zeta_2 \zeta_3 \left(x^3 \zeta_2 \zeta_3^2 + b_2 x^2 \zeta_0 + b_4 x \zeta_0^4 \zeta_1^2 \zeta_2 + b_6 \zeta_0^7 \zeta_1^4 \zeta_2^2\right) . \tag{B.3}$$

The remaining singularities in higher codimension can all be cured by a small resolutions. This can be realized as a sequence of three blowups along the divisors $y = \hat{\zeta}_i = 0$

$$y^2\hat{\zeta}_1\hat{\zeta}_2\hat{\zeta}_3+b_1yx+b_3y\zeta_0^3\zeta_1^2\zeta_2\hat{\zeta}_1^2\hat{\zeta}_2 = x^3\zeta_1\zeta_2^2\zeta_3^3\hat{\zeta}_2\hat{\zeta}_3^2+b_2x^2\zeta_0\zeta_1\zeta_2\zeta_3+b_4x\zeta_0^4\zeta_1^3\zeta_2^2\zeta_3\hat{\zeta}_1^2\hat{\zeta}_2+b_6\zeta_0^7\zeta_1^5\zeta_2^3\zeta_3\hat{\zeta}_1^4\hat{\zeta}_2^2\,. \tag{B.4}$$

Let us rephrase the resolution process just discussed in terms of toric morphisms of the ambient space. The singular situation is described by a hypersurface in a toric variety for which the generators of one-dimensional cones are

$$v_x = (-1,0,0)\,, \qquad v_y = (0,-1,0)\,, \qquad v_{\zeta_0} = (2,3,1)\,. \tag{B.5}$$

The monomials in (B.4) are assigned to the following points in the M-lattice:

Monomial	y^2	b_1xy	$b_3y\zeta_0^3$	x^3	$b_2\zeta_0x^2$	$b_4x\zeta_0^4$	$b_6\zeta_0^7$
Lattice Point	$\begin{pmatrix}-1\\1\\0\end{pmatrix}$	$\begin{pmatrix}0\\0\\-1\end{pmatrix}$	$\begin{pmatrix}1\\0\\0\end{pmatrix}$	$\begin{pmatrix}-2\\1\\0\end{pmatrix}$	$\begin{pmatrix}-1\\1\\-1\end{pmatrix}$	$\begin{pmatrix}0\\1\\0\end{pmatrix}$	$\begin{pmatrix}1\\1\\6\end{pmatrix}$

(B.6)

From the discussion of section 3, it follows that the singularities are then resolved by refining the cone $\langle v_x v_y v_{\zeta_0}\rangle$, by introducing new one-dimensional cones generated by

$$\begin{aligned} v_{\zeta_1} &= (1,2,1) & v_{\hat{\zeta}_1} &= (1,1,1) \\ v_{\zeta_2} &= (0,1,1) & v_{\hat{\zeta}_2} &= (0,0,1) \\ v_{\zeta_3} &= (-1,0,1) & v_{\hat{\zeta}_3} &= (-1,-1,1)\,. \end{aligned} \tag{B.7}$$

These are shown in figure 2. Any triangulation of the polytope spanned by $v_x, v_y, v_{\zeta_0} \cdots v_{\hat{\zeta}_3}$ gives rise to a resolution of (B.1). There are ten triangulations of this polytope, nine of which are realized via successive (weighted) blowups. The power of this point of view is that any toric resolution will introduce the same generators (B.7), so that the weight system of the ambient space is the same for any resolution:

x	y	ζ_0	ζ_1	ζ_2	ζ_3	$\hat{\zeta}_1$	$\hat{\zeta}_2$	$\hat{\zeta}_3$
1	1	1	−1	0	0	0	0	0
1	1	0	1	−1	0	0	0	0
1	1	0	0	1	−1	0	0	0
0	1	0	1	0	0	−1	0	0
0	1	0	0	1	0	0	−1	0
0	1	0	0	0	1	0	0	−1

(B.8)

and what discriminates between different resolutions is only the SR-ideal, which is combinatorially equivalent to a triangulation. Furthermore, it is clear from the above weight system (or, equivalently, the vectors (B.7)), that we will end up with (B.4) for any resolution.

B.2.2 Weighted Blowups and Triangulations

As discussed in sections 3 and 4.3, different sequences of weighted blowups do not necessarily end up with different smooth models, and there are furthermore triangulations which cannot be obtained by any sequence of weighted blowups. In this sections we give some examples for these phenomena in the context of $\mathfrak{su}(7)$ with **21**.

Our first examples concerns two sequences of weighted blowups, which result in the same triangulation and hence in the same phase. Consider the sequences of blowups shown in figure 17. We have only drawn the fiber face part of the fan of the toric ambient space and have indicated which blowup is performed in each step. The points drawn in open circles correspond to homogeneous coordinates that can still be introduced by means of weighted crepant blowups. Note that each $\hat{\zeta}_i$ sits in the cone spanned by y and ζ_i (for all i) and each ζ_i sits in the cone spanned by x and $\hat{\zeta}_{i-1}$ (for $i = 1..3$). The weights of the individual blowups can be recovered from (B.5) and (B.7) together with (3.4).

As a second example, consider the triangulation shown in figure 18. It turns out that this phase can never be reached by a sequence of (weighted) blowups. This can be seen by trying to construct the corresponding blowups. In each step, we have to introduce one of the rays corresponding to the coordinates $\{\zeta_0, \zeta_1, \zeta_2, \zeta_3, \hat{\zeta}_1, \hat{\zeta}_2, \hat{\zeta}_3\}$. In the first step, the only option we have is blowing up $(x, y, \zeta_0; \zeta_3)$, and the corresponding cones are shown in figure 19. The reason is that any other choice would necessarily give rise to cones which are not contained in the triangulation we are aiming for: if we e.g. blow up $(x, y, \zeta_0; \zeta_1)$ we are bound to find a 1-simplex connecting ζ_1 with $\hat{\zeta}_1$, whereas blowing up $(x, y, \zeta_0; \hat{\zeta}_3)$ induces a 1-simplex connecting ζ_0 with $\hat{\zeta}_3$. All other options can be similarly excluded. As a second step after the blowup $(x, y, \zeta_0; \zeta_3)$, we can still introduce any of $\{\zeta_0, \zeta_1, \zeta_2, \hat{\zeta}_1, \hat{\zeta}_2, \hat{\zeta}_3\}$ by a further blowup. As before, any such blowup will either introduce a 1-simplex between ζ_i and $\hat{\zeta}_i$, ζ_{i+1} and $\hat{\zeta}_i$ $(i = 1, 2)$ or $\hat{\zeta}_3$ and ζ_0, all of which do not appear in the triangulation in figure 18.

Note that even though this triangulation cannot be obtained by a sequence of weighted blowups, there is still a well-defined morphism corresponding to the whole resolution (which descends from the corresponding morphism of the ambient space). Furthermore the blown-up ambient space (and hence any algebraic submanifold such as our resolved Calabi-Yau) is still projective after the triangulation by the general argument in section 4.3.

B.2.3 Splitting Rules

Before discussing how fiber components split over the **21** matter curve, we identify which divisors correspond to which Cartan divisors. This is immediate in the present description. We can interpret (B.4) as defining a complex two-dimensional variety. In this case, toric

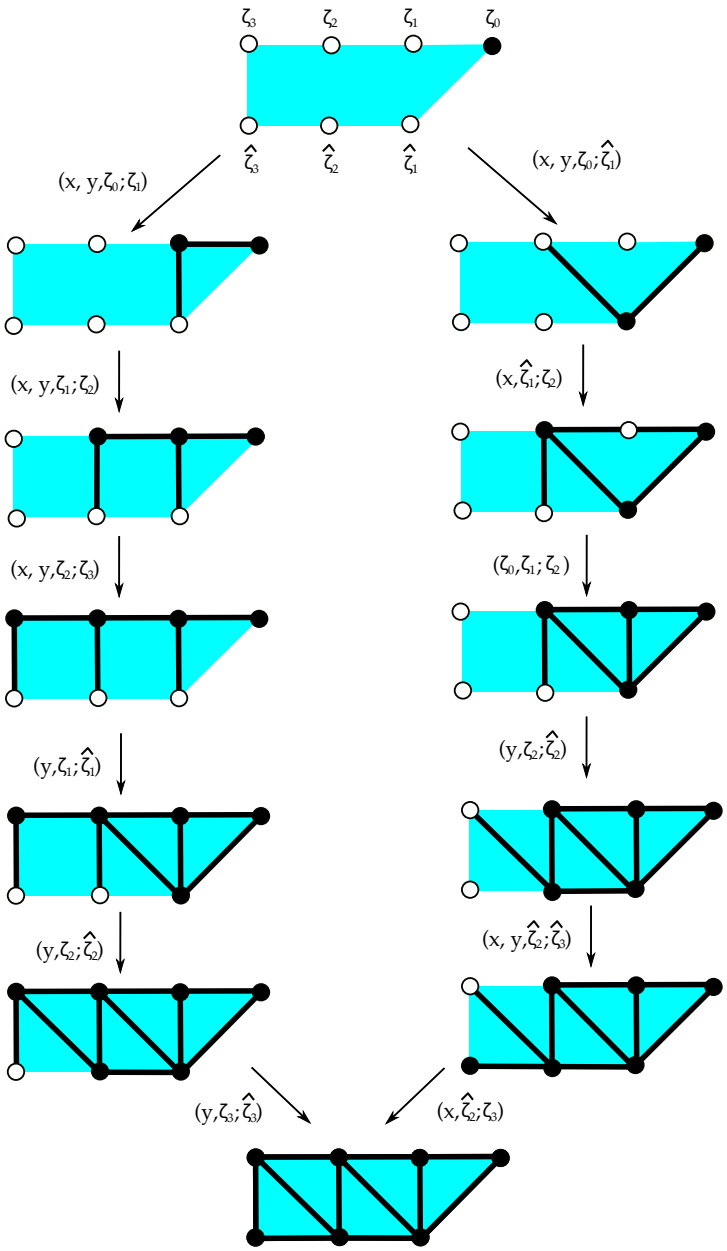

Figure 17: Two different sequences of weighted blowups which end up with the same triangulation and hence the same smooth model.

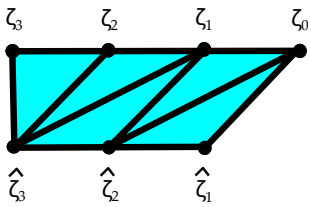

Figure 18: A triangulation which cannot be obtained by a sequence of weighted blowups.

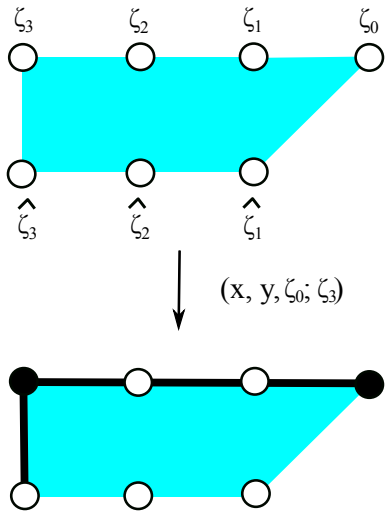

Figure 19: The first step in trying to reach the triangulation shown in figure 18 by a sequence of blowups.

divisors only have a non-zero intersection if the corresponding points are connected along an edge of the polytope. This means we can directly identify

Section	ζ_0	ζ_1	ζ_2	ζ_3	$\hat{\zeta}_1$	$\hat{\zeta}_2$	$\hat{\zeta}_3$
Cartan Divisor	D_{α_0}	D_{α_1}	D_{α_2}	D_{α_3}	D_{α_6}	D_{α_5}	D_{α_4}

(B.9)

In the cases of interest, where we are considering a Calabi-Yau threefold or fourfold, divisors can also meet along loci of higher codimension in the base. We can now find a direct map between the triangulations and the splittings of the fiber components α_i when we go on top of the **10** matter curve at $b_1 = 0$ by using (B.4). The expressions for the different fiber components become

Root	Section	Equation along $b_1 = 0$
α_0	ζ_0	$0 = \hat{\zeta}_2\hat{\zeta}_3\left(y^2\hat{\zeta}_1 - x^3\zeta_1\zeta_2^2\zeta_3^3\right) + b_1yx$
α_1	ζ_1	$0 = y\left(y\hat{\zeta}_1\hat{\zeta}_2\hat{\zeta}_3 + b_1x\right)$
α_2	ζ_2	$0 = y\left(y\hat{\zeta}_1\hat{\zeta}_2\hat{\zeta}_3 + b_1x\right)$
α_3	ζ_3	$0 = y\left(y\hat{\zeta}_1\hat{\zeta}_2\hat{\zeta}_3 + b_3\zeta_0^3\zeta_1^2\zeta_2\hat{\zeta}_1^2\hat{\zeta}_2 + b_1x\right)$
α_4	$\hat{\zeta}_3$	$0 = \zeta_1\zeta_2\left(b_3\zeta_0^3\zeta_1\hat{\zeta}_1^{\,2}\hat{\zeta}_2 - b_2x^2\zeta_0\zeta_3 - b_4x\zeta_0^4\zeta_1^2\zeta_2\zeta_3\hat{\zeta}_1^2\hat{\zeta}_2 - b_6\zeta_0^7\zeta_1^4\zeta_2^2\zeta_3\hat{\zeta}_1^4\hat{\zeta}_2^2\right) + b_1xy$
α_5	$\hat{\zeta}_2$	$0 = \zeta_0\zeta_1\zeta_2\zeta_3b_2x^2 + b_1xy$
α_6	$\hat{\zeta}_1$	$0 = \zeta_1\zeta_2\zeta_3x^2\left(b_2\zeta_0 + x\zeta_2\zeta_3^2\hat{\zeta}_2\hat{\zeta}_3^2\right) + b_1xy$

(B.10)

Note that for any fine triangulation, ζ_1, ζ_2 and ζ_3 cannot vanish simultaneously with y and $\hat{\zeta}_1, \hat{\zeta}_2$ cannot vanish simultaneously with x.

Two divisors D_{α_i} can vanish at the same time if they share a common cone in the fan constructed over simplices of the triangulation. To share a common cone, they must hence be connected by a 1-simplex σ_{ij} on the face F_α. From this, we can read off the following simple rule, already formulated in section 4.3.3, Theorem 4.1:

Let $Z = \{\zeta_0, \zeta_1, \zeta_2, \zeta_3\}$ and $\hat{Z} = \{\hat{\zeta}_1, \hat{\zeta}_2, \hat{\zeta}_3\}$. Then the number of components each divisor splits into over $b_1 = 0$ is equal to the number of 1-simplices which connect it to divisors from the set Z or $\hat{Z}$, whichever does not contain the divisor.

Note that this means that we will find $4 + 4 \cdot 2 = 12$ fiber components of an I_1^* fiber above $b_1 = 0$, as it should be. Furthermore, it is clear which components of the **21** matter surface can be obtained as intersections of which divisors in the different phases. Under this correspondence, the one-simplices internal to F_α can be associated with weights. Let us see how this rule works for the first of the two example triangulations discussed above. In the triangulation shown in figure 17, there is only a single 1-simplex connecting $\zeta_0, \zeta_1, \hat{\zeta}_3$ to the other side of the fiber face. This means that the three fiber components corresponding to α_0, α_1 and α_4 stay irreducible over the locus $b_1 = 0$. In contrast, there is more than a single 1-simplex connecting ζ_2, ζ_3 and $\hat{\zeta}_1, \hat{\zeta}_2$ to the other side, so that $\alpha_2, \alpha_3, \alpha_5$ and α_6 become reducible over $b_1 = 0$ into two and three components, respectively. More precisely,

$$\begin{aligned} F_{0,1,4} &\to F_{0,1,4} \\ F_2 &\to C_a + C_b \\ F_3 &\to C_c + F_4 \\ F_5 &\to C_b + C_c \\ F_6 &\to F_0 + F_1 + C_a \,. \end{aligned} \tag{B.11}$$

The same splitting is found from the box graph as follows directly from our general analysis in section 5.

B.3 Blowdowns and Flops

In this section we explore some flops taking us to phases for which the elliptic fiber is no longer embedded as a toric hypersurface.

As already discussed in section 5.1 for the general case of $\mathfrak{su}(2k+1)$, we rewrite (B.4) in the following two suggestive forms:

$$\begin{aligned} y\hat{y} &= \zeta_1\zeta_2\zeta_3 P \\ xW &= \hat{\zeta}_1\hat{\zeta}_2 S \,, \end{aligned} \tag{B.12}$$

where in this case

$$\begin{aligned}
\hat{y} &= y\hat{\zeta}_1\hat{\zeta}_2\hat{\zeta}_3 + b_1 x + b_3\zeta_0^3\zeta_1^2\zeta_2\hat{\zeta}_1^2\hat{\zeta}_2 \\
P &= x^3\zeta_2\zeta_3^2\hat{\zeta}_2\hat{\zeta}_3^2 + b_2 x^2\zeta_0 + b_4 x\zeta_0^4\zeta_1^2\zeta_2\hat{\zeta}_1^2\hat{\zeta}_2 + b_6\zeta_0^7\zeta_1^4\zeta_2^2\hat{\zeta}_1^4\hat{\zeta}_2^2 \\
W &= x^2\zeta_1\zeta_2^2\zeta_3^3\hat{\zeta}_2\hat{\zeta}_3^2 + b_2 x\zeta_0\zeta_1\zeta_2\zeta_3 + b_4\zeta_0^4\zeta_1^3\zeta_2^2\zeta_3\hat{\zeta}_1^2\hat{\zeta}_2 - b_1 y \\
S &= y^2\hat{\zeta}_3 + b_3 y\zeta_0^3\zeta_1^2\zeta_2\hat{\zeta}_1 - b_6\zeta_0^7\zeta_1^5\zeta_2^3\zeta_3\hat{\zeta}_1^3\hat{\zeta}_2\,.
\end{aligned}$$

The form is suggestive of conifold singularities, however with a fine (i.e. using all points) triangulation of the fiber face spanned by (B.5) and (B.7), the SR ideal always forbids the loci in question. However, for specific triangulations we may perform blow-downs after which a conifold singularity (sitting over $b_1 = 0$ in the fiber) indeed arises due to the factorizations of (B.12). We can then reach the flopped phase in the obvious way by performing the other small resolution. From (B.12) it is already clear that we should consider blowdowns which allow the coordinates $\zeta_1, \zeta_2, \zeta_3$ to vanish with y or $\hat{\zeta}_1, \hat{\zeta}_2$ with x. In fact, it follows from (B.7) that a cone spanned by y, ζ_i contains $\hat{\zeta}_i$ (for all i) and a cone over $x, \hat{\zeta}_i$ contains ζ_{i+1} (for $i = 1, 2$), which nicely corresponds to the factorizations spelled out in (B.12).

As discussed in the main text in section (5.1), not all the corresponding blowdowns give rise to interesting flops. In the following, we discuss the interesting cases in some more detail.

B.3.1 $(y, \zeta_1|\hat{\zeta}_1)$

Let us first consider the blowdowns which result in the fans shown in figure 20.

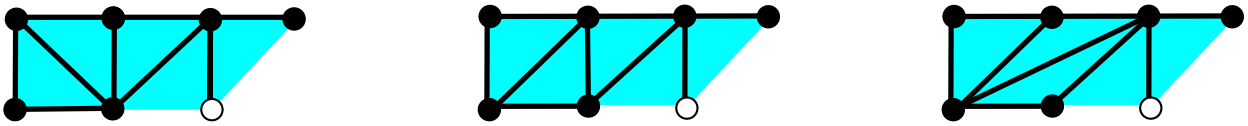

Figure 20: Blowdows of $\hat{\zeta}_1$ for a resolved $\mathfrak{su}(7)$ model. The points correspond to the same homogeneous coordinates as in figure 2.

In both cases, we have fused the cones of the fan such that the ray corresponding to $\hat{\zeta}_1$ is absent. On the level of the toric ambient space this means that we have blown down the divisor $\hat{\zeta}_1 = 0$. There is now a shared cone for y and ζ_1, so that there is now a conifold singularity on the Calabi-Yau at the locus $y = \zeta_1 = \hat{y} = P = 0$ (which implies $b_1 = 0$). On the Calabi-Yau, the divisor $\zeta_1 = 0$ becomes reducible and we associate

$$\begin{aligned}
D_{\alpha_1}: &\qquad \zeta_1 = \hat{y} = 0 \\
D_{\alpha_6}: &\qquad \zeta_1 = y = 0\,.
\end{aligned} \tag{B.13}$$

The reason for this association is that undoing the blowdown again by a blowup $(y, \zeta_1; \hat{\zeta}_1)$, D_{α_6} is mapped to $\hat{\zeta}_1 = 0$ and $\zeta_1 = 0$ (which corresponds to D_{α_1}) implies $\hat{y} = 0$. Note that in

all three cases, the phase before the blowdown was such that D_{α_6} was splitting in precisely two components over $b_1 = 0$.

On the Calabi-Yau, the singular locus is precisely where D_{α_1} and D_{α_6} meet. At the same time, the curve which was present at this locus, i.e. at $\zeta_1 = \hat{\zeta}_1 = 0$, is now gone as well. Hence we conclude the we have blown down the component of D_{α_6} that was shared between D_{α_1} and D_{α_6} over $b_1 = 0$.

We may now reached a flopped phase by performing the second small resolution of the conifold singularity, i.e. by introducing two new coordinates π and δ satisfying the equations

$$\begin{aligned} y\hat{y} &= \zeta_1\zeta_2\zeta_3\pi \\ \delta\pi &= P\,. \end{aligned} \tag{B.14}$$

This gives rise to a new smooth space in which D_{α_1} and D_{α_6} are given by intersecting (B.13) with (B.14). Correspondingly, D_{α_6} is now irreducible over $b_1 = 0$, whereas D_{α_1} receives an extra component over this matter curve. Note that all other divisors and curves remain unperturbed under this operation.

B.3.2 $(x, \hat{\zeta}_2|\zeta_3)$

Similarly, we may blow down ζ_3 reaching the fans shown in figure 21.

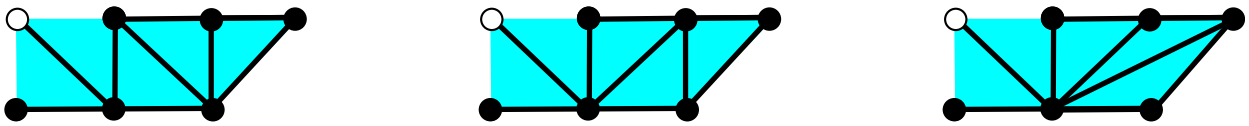

Figure 21: Blowdows of ζ_3 for a resolved $\mathfrak{su}(7)$ model. The points correspond to the same homogeneous coordinates as in figure 2.

The blowdown again gives rise to a conifold singularity over the **21** matter curve and is located at $x = W = \hat{\zeta}_2 = S = 0$. In the blow-down, the divisor $\hat{\zeta}_2$ is reducible and its components are

$$\begin{aligned} D_{\alpha_3}: &\qquad \hat{\zeta}_2 = x = 0 \\ D_{\alpha_5}: &\qquad \hat{\zeta}_2 = W = 0\,. \end{aligned} \tag{B.15}$$

Again, the conifold singularity is at the locus where these two divisors meet. The triangulation of the corresponding smooth phases before the blowdown are such that D_{α_3} has precisely two components over $b_1 = 0$ and the blowdown shrinks the curve which is shared between D_{α_3} and D_{α_5}.

A new resolution corresponding to the flopped phase is obtained by setting

$$\begin{aligned} x\omega &= \hat{\zeta}_2 S \\ \delta\omega &= W\,. \end{aligned} \tag{B.16}$$

The fiber component D_{α_3} is now at $\hat{\zeta}_2 = x = 0$, so that it does not split over $b_1 = 0$ anymore. Similar to what happened before, D_{α_5} gains another component there, so that their total number stays invariant.

B.3.3 $(y, \zeta_1|\hat{\zeta}_1)$ and $(x, \hat{\zeta}_2|\zeta_3)$

As the flops discussed in the last sections were essentially local operations, we can also perform both of them independently (if we start with an appropriate smooth model). There is a single fan for which both ζ_3 and $\hat{\zeta}_1$ can be blown down and flopped. The fan corresponding to the model where both are blown down is shown in figure 22.

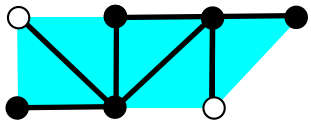

Figure 22: Blowdown of ζ_3 and $\hat{\zeta}_1$ for a resolved $\mathfrak{su}(7)$ model. The points correspond to the same homogeneous coordinates as in figure 2.

B.3.4 Secondary Fiber Face φ

We now describe phases, which can be reached from the partial resolution shown in figure 23, which are obtained after blowing down ζ_2 and ζ_3. This can both be constructed by a sequence of weighted blowups

$$(x, y, \zeta_0; \hat{\zeta}_1) \quad (x, \hat{\zeta}_1, \zeta_0; \zeta_1) \quad (x, y, \hat{\zeta}_1; \hat{\zeta}_2) \quad (x, y, \hat{\zeta}_2; \hat{\zeta}_3)\,. \tag{B.17}$$

or by subsequently blowing down ζ_2 and ζ_3

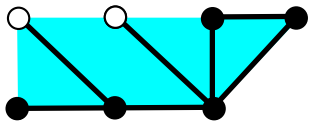

Figure 23: Blowdown of ζ_3 and ζ_2 for a resolved $\mathfrak{su}(7)$ model. The points correspond to the same homogeneous coordinates as in figure 2.

Here, both $\hat{\zeta}_1$ and $\hat{\zeta}_2$ are reducible when intersected with the Calabi-Yau and we identify

$$\begin{aligned} D_{\alpha_2}: &\qquad \hat{\zeta}_1 = x = 0 \\ D_{\alpha_6}: &\qquad \hat{\zeta}_1 = W = 0 \\ D_{\alpha_3}: &\qquad \hat{\zeta}_2 = x = 0 \\ D_{\alpha_5}: &\qquad \hat{\zeta}_2 = W = 0\,. \end{aligned} \tag{B.18}$$

There are now two[10] conifold singularities over $b_1 = 0$, one at $\hat{\zeta}_1 = x = W = S = 0$ and one at $\hat{\zeta}_2 = x = W = S = 0$, which are both apparent from (B.12). In codimension one in the base, our model is already smooth, however.

The different resolutions of this model (besides the ones where we reintroduce the ζ_i) were discussed from a general point of view in section 5. Instead of repeating the analysis, let us work out the details for $\mathfrak{su}(7)$ more explicitly here.

The most obvious way is to resolve by two blowups,

$$(\hat{\zeta}_1, \omega; \delta_1) \quad (\hat{\zeta}_2, \omega; \delta_2)\,, \tag{B.19}$$

where ω is the coordinate associated with W. Hence that the geometry in question is now described by

$$\begin{aligned} x\omega &= \hat{\zeta}_1\hat{\zeta}_2\left(y^2\hat{\zeta}_3 + b_3 y\zeta_0^3\zeta_1^2\hat{\zeta}_1\delta_1 - b_6\zeta_0^7\zeta_1^5\hat{\zeta}_1^3\hat{\zeta}_2\delta_1^3\delta_2\right) \\ \delta_1\delta_2\omega &= x^2\zeta_1\hat{\zeta}_2\hat{\zeta}_3^2\delta_2 + b_2 x\zeta_0\zeta_1 + b_4\zeta_0^4\zeta_1^3\hat{\zeta}_1^2\hat{\zeta}_2\delta_1^2\delta_2 - b_1 y\,. \end{aligned} \tag{B.20}$$

The $\mathbb{C}^*$ actions on the homogeneous coordinates are determined by the weight system

x	y	ζ_0	ζ_1	$\hat{\zeta}_1$	$\hat{\zeta}_2$	$\hat{\zeta}_3$	ω	δ_1	δ_2
1	2	1	0	-1	0	0	2	0	0
1	1	1	-1	0	0	0	1	0	0
1	1	0	0	1	-1	0	1	0	0
1	1	0	0	0	1	-1	1	0	0
0	0	0	0	1	0	0	1	-1	0
0	0	0	0	0	1	0	1	0	-1

(B.21)

We have chosen a basis of $(\mathbb{C}^*)^6$ reflecting the sequence of blowups that were performed.

Before the two blowups introducing δ_1 and δ_2, the SR ideal of the ambient space can be inferred from the diagram in figure 23. After the blowup, (B.19) the SR ideal gains the generators

$$[\omega, \hat{\zeta}_1]\,, [\omega, \hat{\zeta}_2]\,, [\delta_2, \hat{\zeta}_1]\,. \tag{B.22}$$

Furthermore, any set of coordinates which cannot vanish simultaneously with $\hat{\zeta}_1$ ($\hat{\zeta}_1$) is also forbidden to simultaneously vanish with δ_1 (δ_2). In toric language, we may lift the 3-dimensional

[10]The point $x = W = \hat{\zeta}_1 = \hat{\zeta}_2 = 0$ is forbidden due to the SR ideal.

fan with generators (B.5) and (B.7) used above to a four-dimensional fan with the generators

$$\begin{aligned} v_x &= \begin{pmatrix} -1 \\ 0 \\ 0 \\ 0 \end{pmatrix}, v_y = \begin{pmatrix} 0 \\ -1 \\ 0 \\ 0 \end{pmatrix}, v_{\zeta_0} = \begin{pmatrix} 2 \\ 3 \\ 1 \\ 0 \end{pmatrix}, v_{\zeta_1} = \begin{pmatrix} 1 \\ 2 \\ 1 \\ 1 \end{pmatrix}, v_\omega = \begin{pmatrix} 0 \\ 0 \\ 0 \\ 1 \end{pmatrix}, \\ v_{\hat{\zeta}_1} &= \begin{pmatrix} 1 \\ 1 \\ 1 \\ 2 \end{pmatrix}, v_{\hat{\zeta}_2} = \begin{pmatrix} 0 \\ 0 \\ 1 \\ 3 \end{pmatrix}, v_{\hat{\zeta}_3} = \begin{pmatrix} -1 \\ -1 \\ 1 \\ 4 \end{pmatrix}, v_{\delta_1} = \begin{pmatrix} 1 \\ 1 \\ 1 \\ 3 \end{pmatrix}, v_{\delta_2} = \begin{pmatrix} 0 \\ 0 \\ 1 \\ 4 \end{pmatrix}. \end{aligned} \tag{B.23}$$

The 4-dimensional cones of this fan are spanned by

$$\begin{aligned} &\langle x\zeta_1\omega\zeta_0\rangle, \langle xy\hat{\zeta}_3\omega\rangle, \langle\zeta_1\hat{\zeta}_1\zeta_0\delta_1\rangle, \langle\zeta_1\omega\zeta_0\delta_1\rangle, \langle y\hat{\zeta}_1\zeta_0\delta_1\rangle, \langle y\omega\zeta_0\delta_1\rangle, \langle x\zeta_1\hat{\zeta}_1\delta_1\rangle, \langle x\zeta_1\omega\delta_1\rangle, \langle x\hat{\zeta}_2\hat{\zeta}_1\delta_1\rangle, \\ &\langle\hat{\zeta}_2y\hat{\zeta}_1\delta_1\rangle, \langle x\hat{\zeta}_2\hat{\zeta}_3\delta_2\rangle, \langle x\hat{\zeta}_3\omega\delta_2\rangle, \langle\hat{\zeta}_2y\hat{\zeta}_3\delta_2\rangle, \langle y\hat{\zeta}_3\omega\delta_2\rangle, \langle x\hat{\zeta}_2\delta_1\delta_2\rangle, \langle x\omega\delta_1\delta_2\rangle, \langle\hat{\zeta}_2y\delta_1\delta_2\rangle, \langle y\omega\delta_1\delta_2\rangle\,. \end{aligned} \tag{B.24}$$

The way these cones fit together can be visualized in the cone diagram shown in figure 24. The fiber components over $b_1 = 0$ become:

Root	Section	over $b_1 = 0$
α_0	ζ_0	$x\omega = \hat{\zeta}_1\hat{\zeta}_2y^2\hat{\zeta}_3$
		$\delta_1\delta_2\omega = x^2\zeta_1\hat{\zeta}_2\hat{\zeta}_3^2\delta_2$
α_1	ζ_1	$x\omega = \hat{\zeta}_1\hat{\zeta}_2y^2\hat{\zeta}_3$
		$\delta_1\delta_2\omega = 0$
α_2	$\hat{\zeta}_1$	$x\omega = 0$
		$\delta_1\delta_2\omega = b_2x\zeta_0\zeta_1$
α_3	$\hat{\zeta}_2$	$x\omega = 0$
		$\delta_1\delta_2\omega = b_2x\zeta_0\zeta_1$
α_4	$\hat{\zeta}_3$	$x\omega = \hat{\zeta}_1\hat{\zeta}_2\left(b_3y\zeta_0^3\zeta_1^2\hat{\zeta}_1\delta_1 - b_6\zeta_0^7\zeta_1^5\hat{\zeta}_1^3\hat{\zeta}_2\delta_1^3\delta_2\right)$
		$\delta_1\delta_2\omega = b_2x\zeta_0\zeta_1 + b_4\zeta_0^4\zeta_1^3\hat{\zeta}_1^2\hat{\zeta}_2\delta_1^2\delta_2$
α_5	δ_2	$x\omega = \hat{\zeta}_1\hat{\zeta}_2\left(y^2\hat{\zeta}_3 + b_3y\zeta_0^3\zeta_1^2\hat{\zeta}_1\delta_1\right)$
		$0 = b_2x\zeta_0\zeta_1$
α_6	δ_1	$x\omega = \hat{\zeta}_1\hat{\zeta}_2y^2\hat{\zeta}_3\,.$
		$0 = x\zeta_1\left(\hat{\zeta}_2\hat{\zeta}_3^2\delta_2 + b_2\zeta_0\right)$

(B.25)

Let us now discuss the splitting of the various components in turn.

- Even though the expression for F_0 can be solved by setting three homogeneous coordinates to zero, all such options are forbidden by the SR ideal. Correspondingly, F_0 stays irreducible.

- The second equation defining F_1 seemingly splits into three components. However, $[\delta_2, \zeta_1]$ is in the SR ideal, as are $[\zeta_1, \omega, \hat{\zeta}_1]$, $[\zeta_1, \omega, \hat{\zeta}_2]$, $[\zeta_1, \omega, \hat{\zeta}_3]$ and $[\zeta_1, \omega, y]$. Hence F_1 sits at $\zeta_1 = \delta_1 = x\omega - \hat{\zeta}_1\hat{\zeta}_2 y^2 \hat{\zeta}_3 = 0$ and is irreducible.

- For F_2, it is important that $[\omega, \hat{\zeta}_1]$ and $[\hat{\zeta}_1, \delta_2]$ are in the SR ideal. This forces $x = \delta_1 = 0$ and makes F_2 irreducible over $b_1 = 0$.

- The first equation describing the fiber component F_3 again forces $x = 0$ as $[\omega, \hat{\zeta}_2]$ is in the SR ideal. Over $b_1 = 0$, this leaves the two components at $\delta_1 = 0$ and $\delta_2 = 0$.

- The component F_4 stays irreducible over $b_1 = 0$ as $[\omega, \hat{\zeta}_1]$ and $[\omega, \hat{\zeta}_2]$ are in the SR ideal.

- F_5 splits into the two components $x = \hat{\zeta}_2 = 0$ and $x = y^2\hat{\zeta}_3 + b_3 y \zeta_0^3 \zeta_1^2 \hat{\zeta}_1 \delta_1 = 0$

- F_6 splits into the four components $\zeta_1 = 0$, $\hat{\zeta}_2\hat{\zeta}_3^2\delta_2 + b_2\zeta_0 = 0$ as well as $x = \hat{\zeta}_1 = 0$, $x = \hat{\zeta}_2 = 0$.

In summary, we hence get five extra components over $b_1 = 0$, as expected, and the splitting can be summarized as

$$\begin{aligned} F_3 &\to C_a + C_b \\ F_5 &\to C_a + C_c \\ F_6 &\to F_1 + F_2 + C_b + C_d \,. \end{aligned} \tag{B.26}$$

The corresponding fiber face and box graph is the case ρ_1 shown in figure 24.

From the general discussion one expects that there should be two more phases described by (B.20), for which the face containing the coordinates δ_1, δ_2 and $\hat{\zeta}_1, \hat{\zeta}_2, \hat{\zeta}_3$ is triangulated differently. These remaining triangulations and box graphs ρ_2 and ρ_3 are shown in figure 24.

The case ρ_2 is obtained by performing a flop on the resolution associated to ρ_1. From the box graph, this corresponds to sign-changing the weight $L_4 + L_6$, giving rise to the box graph ρ_2 in figure 24. In particular this means that the curve C_a, which is at $\hat{\zeta}_2 = \delta_2 = 0$ (from which $x = 0$ follows), and carries weight $L_4 + L_5$, ceases to be extremal. A glance at the corresponding fiber face, shows that this curve corresponds to the line connecting δ_2 with $\hat{\zeta}_2$. We can perform a flop in which this 1-simplex is replaced by a one-simplex connecting δ_1 and $\hat{\zeta}_3$, as shown in figure 24, where the fiber face ρ is triangulated now as in ρ_2. The ambient space of the flopped phase hence has the same generators (B.23), but the 4-dimensional cones are now

$$\begin{aligned} &\langle x\zeta_1\omega\zeta_0\rangle, \langle xy\hat{\zeta}_3\omega\rangle, \langle\zeta_1\hat{\zeta}_1\zeta_0\delta_1\rangle, \langle\zeta_1\omega\zeta_0\delta_1\rangle, \langle y\hat{\zeta}_1\zeta_0\delta_1\rangle, \langle y\omega\zeta_0\delta_1\rangle, \langle x\zeta_1\hat{\zeta}_1\delta_1\rangle, \langle x\zeta_1\omega\delta_1\rangle, \langle x\hat{\zeta}_2\hat{\zeta}_1\delta_1\rangle, \\ &\langle\hat{\zeta}_2 y\hat{\zeta}_1\delta_1\rangle, \langle x\hat{\zeta}_2\hat{\zeta}_3\delta_1\rangle, \langle x\hat{\zeta}_3\omega\delta_2\rangle, \langle\hat{\zeta}_2 y\hat{\zeta}_3\delta_1\rangle, \langle y\hat{\zeta}_3\omega\delta_2\rangle, \langle x\hat{\zeta}_3\delta_1\delta_2\rangle, \langle x\omega\delta_1\delta_2\rangle, \langle y\hat{\zeta}_3\delta_1\delta_2\rangle, \langle y\omega\delta_1\delta_2\rangle \,. \end{aligned} \tag{B.27}$$

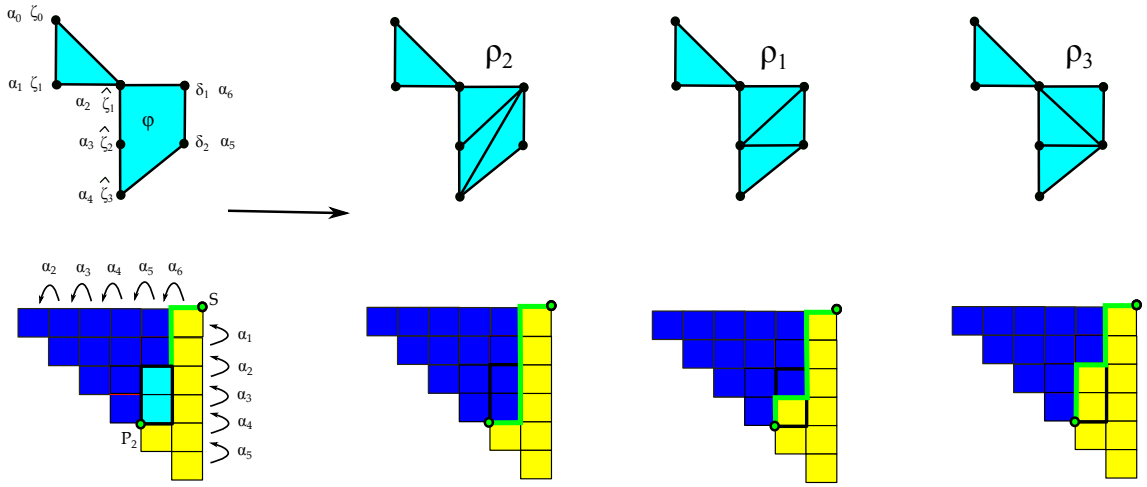

Figure 24: Triangulations and box graphs for the secondary fiber faces of type shown in figure 11 and 12. for $\mathfrak{su}(7)$. Each triangulation ρ_i of the secondary fiber face φ corresponds to a sign assignment/colouring of the turquoise region in the box graph shown in the second line. Note that there are three more colourings of the box graphs, which however correspond to standard toric triangulations of figure 5.

This means that we have replaced $\langle \hat{\zeta}_2, \hat{\zeta}_3, \delta_2 \rangle$, $\langle \hat{\zeta}_2, \delta_1, \delta_2 \rangle$ by $\langle \hat{\zeta}_2, \hat{\zeta}_3, \delta_1 \rangle$, $\langle \hat{\zeta}_3 \delta_1 \delta_2 \rangle$.

The elliptic fibration and the fiber components are of course still given by the same equations (B.20). When we discuss the splitting over the locus $b_1 = 0$, however, the components F_3 and F_5 are still irreducible as now $[\delta_2, \hat{\zeta}_2]$ is in the SR ideal.

The components F_4 and F_6 now each have an extra component at $\hat{\zeta}_3 = \delta_1 = 0$. The splittings are hence

$$\begin{aligned} F_4 &\to C_e + C_f \\ F_6 &\to F_1 + F_2 + F_3 + C_e + C_d \,, \end{aligned} \tag{B.28}$$

which precisely corresponds to the fiber face ρ_2 and associated box graph in figure 24.

Finally, to describe the resolution ρ_3 in figure 24, consider again ρ_1 and flop the 1-simplex connecting δ_1 with $\hat{\zeta}_2$ by replacing it with a 1-simplex connecting δ_2 with $\hat{\zeta}_2$. Not surprisingly, in this flop the curve shared by D_{α_3} and D_{α_6} is blown down and a new curve, now shared between D_{α_2} and D_{α_5} emerges. Hence we expect this geometry to be identical to the one described in section B.3.2 by the diagram on the left of figure 21.

B.3.5 Flop to Ternary Fiber Face

The box graph, which in terms of our nomenclature of fiber faces in the main text, see section 6 corresponds to the ternary fiber face (which for $\mathfrak{su}(7)$ is the final layer) is given by

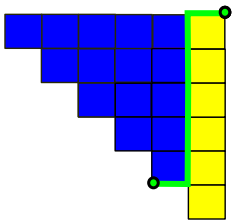

(B.29)

Like in section 6.1, we can determine this phase by a flop from the phase associated to ρ_2 5.

Consider the equation of the phase (B.28) corresponding to the secondary fiber face triangulation ρ_2

$$\begin{aligned} \hat{\zeta}_1\hat{\zeta}_2\left(-b_6\delta_1^3\delta_2\zeta_1^5\zeta_0^7\hat{\zeta}_1^3\hat{\zeta}_2 + b_3\delta_1\zeta_1^2\zeta_0^3 y\hat{\zeta}_1 + y^2\hat{\zeta}_3\right) - x\omega = 0 \\ b_4\delta_1^2\delta_2\zeta_1^3\zeta_0^4\hat{\zeta}_1^2\hat{\zeta}_2 + b_2\zeta_1\zeta_0 x - b_1 y - \delta_1\delta_2\omega + \delta_2\zeta_1 x^2\hat{\zeta}_2\hat{\zeta}_3^2 = 0\,. \end{aligned} \tag{B.30}$$

with the projective relations

$$\begin{aligned} \left\{\zeta_0, \delta_2\hat{\zeta}_2\hat{\zeta}_3\right\}, \{y, \zeta_1\}, \left\{\zeta_1, \delta_2\hat{\zeta}_2\hat{\zeta}_3\right\}, \left\{\omega, \hat{\zeta}_1\hat{\zeta}_2\right\}, \left\{\hat{\zeta}_1, \delta_2\hat{\zeta}_3\right\}, \\ \left\{\hat{\zeta}_2, \delta_2\right\}, \left\{x, \zeta_0, \delta_1\hat{\zeta}_1\right\}, \left\{x, y, \delta_1\delta_2\zeta_0\hat{\zeta}_1\hat{\zeta}_2\right\}, \left\{\omega, \hat{\zeta}_3, \delta_1\right\}\,. \end{aligned} \tag{B.31}$$

As $\omega = 0$ intersects the exceptional curves in points, and is not going to play any role in the flop.

We thus assume that $\omega \neq 0$ and solve the first equation for x and insert it into the second equation, so that the geometry is now the hypersurface

$$\begin{aligned} 0 = {} & b_2\zeta_0\zeta_1\omega\hat{\zeta}_1\hat{\zeta}_2\left(-b_6\delta_1^3\delta_2\zeta_1^5\zeta_0^7\hat{\zeta}_1^3\hat{\zeta}_2 + b_3\delta_1\zeta_1^2\zeta_0^3 y\hat{\zeta}_1 + y^2\hat{\zeta}_3\right) \\ & + \delta_2\zeta_1\hat{\zeta}_1^2\hat{\zeta}_2^3\hat{\zeta}_3^2\left(-b_6\delta_1^3\delta_2\zeta_1^5\zeta_0^7\hat{\zeta}_1^3\hat{\zeta}_2 + b_3\delta_1\zeta_1^2\zeta_0^3 y\hat{\zeta}_1 + y^2\hat{\zeta}_3\right)^2 + \omega^2(b_4\delta_1^2\delta_2\zeta_0^4\zeta_1^3\hat{\zeta}_1^2\hat{\zeta}_2 - b_1 y - \delta_1\delta_2\omega)\,. \end{aligned} \tag{B.32}$$

One can easily check that the curve that has to be flopped to reach the final phase is given by

$$\hat{\zeta}_3 = b_1 = 0 \;: \qquad \delta_1 s_3 = 0\,, \tag{B.33}$$

where $\delta_1 = 0$ is the component that needs to be retained, and s_3 is defined in (B.34). We will now rewrite the equations in new coordinates, and show explicitly how a conifold equation

emerges. This is very similar to the flops in [5]. Define the new coordinates

$$\begin{aligned}
s_1 &= \hat{\zeta}_2 \\
s_2 &= \delta_1 s_1 \\
s_3 &= -b_2 b_6 \delta_1^2 \delta_2 \zeta_1^6 \zeta_0^8 \omega \hat{\zeta}_1^4 \hat{\zeta}_2^2 + b_6^2 \delta_1^5 \delta_2^3 \zeta_1^{11} \zeta_0^{14} \hat{\zeta}_1^8 \hat{\zeta}_2^5 \hat{\zeta}_3^2 + \omega \left(\delta_2 \omega \left(b_4 \delta_1 \zeta_0^4 \zeta_1^3 \hat{\zeta}_1^2 \hat{\zeta}_2 - \omega \right) + b_2 b_3 \zeta_1^3 \zeta_0^4 y \hat{\zeta}_1^2 \hat{\zeta}_2 \right) \\
s_4 &= \delta_1 s_3 \,.
\end{aligned} \tag{B.34}$$

The equation (B.32) can then be rewritten in terms of solely these coordinates (in particular no explicit dependence on δ_1)

$$\begin{aligned}
s_4 = &- b_2 \zeta_0 \zeta_1 s_1 y^2 \omega \hat{\zeta}_1 \hat{\zeta}_3 + b_1 y \omega^2 \\
&+ y \delta_2 \zeta_1 \hat{\zeta}_1^2 \hat{\zeta}_3^2 \left(b_3 \zeta_1^2 \zeta_0^3 s_2 \hat{\zeta}_1 + s_1 y \hat{\zeta}_3 \right) \left(2 b_6 \delta_2 \zeta_1^5 \zeta_0^7 s_2^3 \hat{\zeta}_1^3 - b_3 \zeta_1^2 \zeta_0^3 s_1 s_2 y \hat{\zeta}_1 - s_1^2 y^2 \hat{\zeta}_3 \right) \,,
\end{aligned} \tag{B.35}$$

with the extra condition, rewritten in terms of s_1 and s_2,

$$s_3 = b_6^2 \delta_2^3 \zeta_1^{11} \zeta_0^{14} s_2^5 \hat{\zeta}_1^8 \hat{\zeta}_3^2 - b_2 b_6 \delta_2 \zeta_1^6 \zeta_0^8 s_2^2 \hat{\zeta}_1^4 \omega + b_4 \delta_2 \zeta_1^3 \zeta_0^4 s_2 \hat{\zeta}_1^2 \omega^2 + b_2 b_3 \zeta_1^3 \zeta_0^4 s_1 y \hat{\zeta}_1^2 \omega - \delta_2 \omega^3 \,, \tag{B.36}$$

and this is equivalent to the initial equation in the patch by imposing the condition, which makes manifest the relation among the new coordinates

$$s_1 s_4 = s_2 s_3 \,, \tag{B.37}$$

which is exactly the conifold equation. Note that δ_1 does not appear in these equations any longer.

We can think of this equation as the resolution of the conifold with

$$s_1 \rho_1 = s_2 \rho_2 \,, \qquad s_3 \rho_1 = s_4 \rho_2 \,, \tag{B.38}$$

where $[\rho_1, \rho_2]$ are projective coordinates on a $\mathbb{P}^1$ and we considered the patch $\rho_1 \neq 0$ where $\delta_1 = \rho_2 / \rho_1$.

The flop of the conifold is now obtained by

$$s_1 \xi_1 = s_3 \xi_2 \,, \qquad s_4 \xi_2 = s_2 \xi_1 \,. \tag{B.39}$$

Consider the patch $\xi_1 \neq 0$ and introduce $\xi = \xi_2 / \xi_1$, and replacing s_1 and s_2 accordingly yields

$$\begin{aligned}
s_4 = &- y \delta_2 \zeta_1 \xi^3 \hat{\zeta}_1^2 \hat{\zeta}_3^2 \left(b_3 \zeta_1^2 \zeta_0^3 s_4 \hat{\zeta}_1 + s_3 y \hat{\zeta}_3 \right) \left(s_3 y \left(b_3 \zeta_1^2 \zeta_0^3 s_4 \hat{\zeta}_1 + s_3 y \hat{\zeta}_3 \right) - 2 b_6 \delta_2 \zeta_0^7 \zeta_1^5 \xi s_4^3 \hat{\zeta}_1^3 \right) \\
&+ b_2 \zeta_0 \zeta_1 \xi s_3 y^2 \omega \hat{\zeta}_1 \hat{\zeta}_3 - b_1 y \omega^2 \\
s_3 = &\, b_6^2 \delta_2^3 \zeta_1^{11} \zeta_0^{14} \xi^5 s_4^5 \hat{\zeta}_1^8 \hat{\zeta}_3^2 - b_2 b_6 \delta_2 \zeta_1^6 \zeta_0^8 \xi^2 s_4^2 \hat{\zeta}_1^4 \omega + b_4 \delta_2 \zeta_1^3 \zeta_0^4 \xi s_4 \hat{\zeta}_1^2 \omega^2 + b_2 b_3 \zeta_1^3 \zeta_0^4 \xi s_3 y \hat{\zeta}_1^2 \omega - \delta_2 \omega^3 \,.
\end{aligned} \tag{B.40}$$

Let us consider the various components along $b_1 = 0$ – we have used the SR ideal to eliminate coordinates that cannot vanish at the same time:

$$\begin{aligned}
\zeta_1 = 0: &\quad s_4 = \delta_2 + s_3 = 0 \\
\hat{\zeta}_1 = 0: &\quad s_4 = \delta_2 + s_3 = 0 \\
\xi = 0: &\quad s_4 = \delta_2 + s_3 = 0 \\
s_3 = 0: &\quad s_4 \left(2 b_3 b_6 \delta_2^2 \zeta_0^{10} \zeta_1^8 \xi^4 s_4^3 y \hat{\zeta}_1^6 \hat{\zeta}_3^2 - 1\right) = 0 \\
&\quad \delta_2 \left(b_6^2 \delta_2^2 \zeta_1^{11} \zeta_0^{14} \xi^5 s_4^5 \hat{\zeta}_1^8 \hat{\zeta}_3^2 - b_2 b_6 \zeta_1^6 \zeta_0^8 \xi^2 s_4^2 \hat{\zeta}_1^4 + b_4 \zeta_1^3 \zeta_0^4 \xi s_4 \hat{\zeta}_1^2 - 1\right) = 0 \\
\hat{\zeta}_3 = 0: &\quad s_4 = s_3 \left(b_2 b_3 \zeta_0^4 \zeta_1^3 \xi y \hat{\zeta}_1^2 - 1\right) - \delta_2 = 0 \\
\delta_2 = 0: &\quad b_2 \zeta_0 \zeta_1 \xi s_3 \omega y^2 \hat{\zeta}_1 \hat{\zeta}_3 + s_4 = 0 \\
&\quad s_3 \left(b_2 b_3 \zeta_0^4 \zeta_1^3 \xi y \hat{\zeta}_1^2 - 1\right) = 0 \\
s_4 = 0: &\quad \zeta_1 \xi s_3 \hat{\zeta}_1 \hat{\zeta}_3 \left(b_2 \zeta_0 \omega + \xi^2 s_3^3 \hat{\zeta}_1 \hat{\zeta}_3^3 \left(b_2 b_3 \zeta_0^4 \zeta_1^3 \xi \hat{\zeta}_1^2 - 1\right)\right) = 0 \,.
\end{aligned} \tag{B.41}$$

Note that $s_3 = \delta_2 = 0$, which naively looks like an additional component, is in fact not allowed because it implies $\hat{\zeta}_2 = 0$ from the definition of s_3, which is however not consistent with the projective relations. All components are irreducible except $s_4 = 0$, which corresponds to F_6. It can be traced back through the flop to $\delta_1 = 0$ and splits into six components, which is exactly as required from the final phase. This completes the correspondence between the geometric realizations of resolutions and box graphs.

References

[1] C. Vafa, *Evidence for F-Theory*, *Nucl. Phys.* **B469** (1996) 403–418, [hep-th/9602022]. 1

[2] D. R. Morrison and C. Vafa, *Compactifications of F-Theory on Calabi–Yau Threefolds – I*, *Nucl. Phys.* **B473** (1996) 74–92, [hep-th/9602114]. 1, 2.3

[3] D. R. Morrison and C. Vafa, *Compactifications of F-Theory on Calabi–Yau Threefolds – II*, *Nucl. Phys.* **B476** (1996) 437–469, [hep-th/9603161]. 1, 2.3

[4] H. Hayashi, C. Lawrie, D. R. Morrison, and S. Schafer-Nameki, *Box Graphs and Singular Fibers*, *JHEP* **1405** (2014) 048, [1402.2653]. 1, 2, 2.1, 1, 2.2, 2.3, 7, B.1

[5] H. Hayashi, C. Lawrie, and S. Schafer-Nameki, *Phases, Flops and F-theory: SU(5) Gauge Theories*, *JHEP* **1310** (2013) 046, [1304.1678]. 1, 4.2, B.3.5

[6] A. P. Braun and S. Schafer-Nameki, *Box Graphs and Resolutions I*, 1407.3520. 1, 2.2, 3, 7

[7] C. Lawrie, S. Schafer-Nameki, and J.-M. Wong, *F-theory and All Things Rational: Surveying U(1) Symmetries with Rational Sections*, 1504.05593. 1, 2, 2.3, 2.3

[8] M. Esole, S.-H. Shao, and S.-T. Yau, *Singularities and Gauge Theory Phases*, 1402.6331. 1

[9] M. Esole, S.-H. Shao, and S.-T. Yau, *Singularities and Gauge Theory Phases II*, 1407.1867. 1

[10] K. A. Intriligator, D. R. Morrison, and N. Seiberg, *Five-dimensional supersymmetric gauge theories and degenerations of Calabi-Yau spaces*, *Nucl.Phys.* **B497** (1997) 56–100, [hep-th/9702198]. 1

[11] O. Aharony, A. Hanany, K. A. Intriligator, N. Seiberg, and M. Strassler, *Aspects of N=2 supersymmetric gauge theories in three-dimensions*, *Nucl.Phys.* **B499** (1997) 67–99, [hep-th/9703110]. 1

[12] J. de Boer, K. Hori, and Y. Oz, *Dynamics of N=2 supersymmetric gauge theories in three-dimensions*, *Nucl.Phys.* **B500** (1997) 163–191, [hep-th/9703100]. 1

[13] D.-E. Diaconescu and S. Gukov, *Three-dimensional N=2 gauge theories and degenerations of Calabi-Yau four folds*, *Nucl.Phys.* **B535** (1998) 171–196, [hep-th/9804059]. 1

[14] T. W. Grimm and H. Hayashi, *F-theory fluxes, Chirality and Chern-Simons theories*, *JHEP* **1203** (2012) 027, [1111.1232]. 53 pages, 5 figures/ v2: typos corrected, minor improvements. 1

[15] S. Krippendorf, S. Schafer-Nameki, and J.-M. Wong, *Froggatt-Nielsen meets Mordell-Weil: A Phenomenological Survey of Global F-theory GUTs with U(1)s*, 1507.05961. 1

[16] M. Esole and S.-T. Yau, *Small resolutions of SU(5)-models in F-theory*, 1107.0733. 1, 4.2

[17] J. Marsano and S. Schafer-Nameki, *Yukawas, G-flux, and Spectral Covers from Resolved Calabi-Yau's*, *JHEP* **1111** (2011) 098, [1108.1794]. 1, 4.2

[18] A. P. Braun, A. Collinucci, and R. Valandro, *G-flux in F-theory and algebraic cycles*, *Nucl.Phys.* **B856** (2012) 129–179, [1107.5337]. 55 pages, 1 figure/ added refs, corrected typos. 1

[19] S. Krause, C. Mayrhofer, and T. Weigand, *G_4 flux, chiral matter and singularity resolution in F-theory compactifications*, *Nucl.Phys.* **B858** (2012) 1–47, [1109.3454]. 53 pages, 2 figures. 1

[20] D. R. Morrison and W. Taylor, *Matter and singularities*, *JHEP* **01** (2012) 022, [1106.3563]. 1

[21] M. Kuntzler and S. Schafer-Nameki, *G-flux and Spectral Divisors*, *JHEP* **1211** (2012) 025, [1205.5688]. 1

[22] C. Lawrie and S. Schafer-Nameki, *The Tate Form on Steroids: Resolution and Higher Codimension Fibers*, *JHEP* **1304** (2013) 061, [1212.2949]. 1, 4.1, 4.2, B.2.1

[23] V. Braun, T. W. Grimm, and J. Keitel, *Complete Intersection Fibers in F-Theory*, *JHEP* **1503** (2015) 125, [1411.2615]. 1

[24] M. Bershadsky, K. A. Intriligator, S. Kachru, D. R. Morrison, V. Sadov, *et. al.*, *Geometric singularities and enhanced gauge symmetries*, *Nucl.Phys.* **B481** (1996) 215–252, [hep-th/9605200]. 1, 4.1

[25] S. Katz, D. R. Morrison, S. Schafer-Nameki, and J. Sully, *Tate's algorithm and F-theory*, *JHEP* **1108** (2011) 094, [1106.3854]. 1, 4.1

[26] P. Candelas and A. Font, *Duality between the webs of heterotic and type II vacua*, *Nucl.Phys.* **B511** (1998) 295–325, [hep-th/9603170]. 1, 3.3, 4.3.1

[27] O. Debarre, *Higher-dimensional algebraic geometry*. Universitext. Springer-Verlag, New York, 2001. 2.3

[28] V. I. Danilov, *The geometry of toric varieties*, *Russian Mathematical Surveys* **33** (1978), no. 2 97. 3

[29] W. Fulton, *Introduction to toric varieties*. Princeton University Press, Princeton, 1993. 3, 3, 3.4, 5

[30] D. Cox, J. Little, and H. Schenck, *Toric Varieties*. Graduate studies in mathematics. American Mathematical Society, 2011. 3

[31] M. Kreuzer, *Toric geometry and Calabi-Yau compactifications*, *Ukr.J.Phys.* **55** (2010) 613–625, [hep-th/0612307]. 3, 3.2

[32] V. Bouchard, *Lectures on complex geometry, Calabi-Yau manifolds and toric geometry*, hep-th/0702063. 3

[33] E. Perevalov and H. Skarke, *Enhanced gauged symmetry in type II and F theory compactifications: Dynkin diagrams from polyhedra*, *Nucl.Phys.* **B505** (1997) 679–700, [hep-th/9704129]. 3.3, 4.3.1

[34] V. Bouchard and H. Skarke, *Affine Kac-Moody algebras, CHL strings and the classification of tops*, *Adv.Theor.Math.Phys.* **7** (2003) 205–232, [hep-th/0303218]. 3.3

[35] C. Lawrie and S. Schafer-Nameki, *In progress.* 4.4

[36] C. Curto and D. R. Morrison, *Threefold flops via matrix factorization*, *J. Algebraic Geom.* **22** (2013), no. 4 599–627. 7

[37] A. Grassi, J. Halverson, and J. L. Shaneson, *Matter From Geometry Without Resolution*, *JHEP* **1310** (2013) 205, [1306.1832]. 7

[38] A. Collinucci and R. Savelli, *F-theory on singular spaces*, 1410.4867. 7

[39] P. S. Aspinwall, B. R. Greene, and D. R. Morrison, *Calabi-Yau moduli space, mirror manifolds and space-time topology change in string theory*, *Nucl. Phys.* **B416** (1994) 414–480, [hep-th/9309097]. 7

[40] D. A. Cox and S. Katz, *Mirror symmetry and algebraic geometry.* AMS, 2000. 7